Determination of the aerosol direct effect over the East China Sea using ground-based remote sensing and aircraft observation data

Pradeep Khatri[1]*, Tamio Takamura[1], Akhiro Yamazaki[2], Yutaka Kondo[3], Atsushi Shimizu[4], and Nobuo Sugimoto[4]

[1]Center for Environmental Remote Sensing, Chiba University, 1-33 Yayoi, Inage, Chiba, Japan
[2] Meteorological Research Institute, 1-1 Nagamine, Tsukuba, Ibaraki 305-0052, Japan
[3]Department of Earth and Planetary Science, The University of Tokyo, 7-3-1 Hongo, Bunkyo, Tokyo 113-0033, Japan
[4]National Institute for Environmental Studies, 16-2 Onogawa, Tsukuba, Ibaraki 305-8506, Japan

Corresponding author. Tel.: +81 43 290 3869; Fax: +81 43 290 3857, Email address: pradeep.nep@gmail.com (P. Khatri)

Meteorological and aerosol data observed from aircraft over the East China Sea region as well as aerosol radiative parameters and surface irradiances observed by ground-based remote sensing instruments were input a radiative transfer model to study the vertical profiles of aerosol radiative forcing and the aerosol heating rate over the study region. The results showed that in spring, some aerosol layers above the boundary layer can have a strong heating effect comparable to that of aerosols within the boundary layer. This result suggests that aerosols above the boundary layer can have important effects on the atmospheric heat budget over the East China Sea region in spring.

Keywords: Aerosol particles; Aerosol optical thickness; Single scattering albedo; Aerosol radiative forcing

1. Introduction

Despite the important effects of East Asian aerosols on climate change, how those aerosols are linked with regional and global climate change, a major scientific question, is not well understood because of their spatial and temporal variations as well as the complexity of their physical, chemical, and optical characteristics. Efforts are being made by the scientific community to understand the characteristics of East Asian aerosols and their roles in the climate system. One important reason for the poor understanding of the direct and indirect effects of East Asian aerosols on climate is the inadequate understanding of the vertical profiles of aerosol optical parameters and aerosol radiative forcing. Widely used instruments for aerosol observation such as the Prede sky radiometer and the CIMEL sun photometer can provide information about only columnar aerosols, and lidar systems are capable of providing only limited information about the vertical profile of aerosols. The most important parameter for estimating aerosol radiative forcing, single scattering albedo (SSA), cannot be measured directly. Implementation of the vertical profiles of SSA and other radiative parameters in radiative transfer models is necessary for precise calculation of the aerosol direct effect. Aircraft observations are very useful for understanding the vertical distribution of aerosols and other atmospheric parameters. This study utilized simultaneous aircraft observation data and ground-based remote sensing data to investigate the vertical profiles of aerosol radiative parameters and the aerosol direct effect over the East China Sea in spring.

2. Data and study method

We used observation data collected at the Fukue-Jima Island (32.752°N, 128.682°E) on 30 March and 5 April 2009. Vertical profiles of black carbon concentration and relative humidity were observed by aircraft over Fukue-jima, and spectral aerosol optical thickness and SSA at wavelengths of 399.1, 499.0, 675.6, 870.6, and 1020.2 nm were retrieved by using spectral irradiances measured with an MS-700 spectroradiometer and the algorithm of Khatri et al. (2012: Ref. 1). Further, we used the spectral asymmetry parameter (ASY) retrieved by a sky radiometer (Manufacture: PREDE Co. Ltd., Japan, model: POM-02) as well as vertical profiles of the aerosol extinction coefficient and yellow sand index (YSI) at 532 nm measured by a lidar. YSI is defined as the contribution of non-spherical (dust) aerosol optical thickness to the total aerosol optical thickness [2].

By assuming that the three types of aerosols, namely water soluble, dust, and black carbon, were externally mixed, we derived the vertical profiles of the extinction coefficient, SSA, and ASY at the wavelengths of 399.1, 499.0, 675.6, 870.6, and 1020.2 nm in such a way that the integrated vertical profiles of those optical parameters would produce the best agreement with the columnar values measured at ground level by the MS-700 spectroradiometer and the sky radiometer. For this purpose, we used the optical data given in the Optical Properties of Aerosols and Clouds (OPAC) software [3]. Finally, vertical profiles of the extinction coefficient, SSA, and ASY as well as the columnar water vapor content measured by a microwave radiometer and surface reflectance measured by MODIS were input into the Santa Barbara DISORT atmospheric radiative transfer (SBDART) model [4] to estimate the vertical profiles of aerosol direct radiative forcing and of the heating rate.

3. Results and discussion

In Figure 1, the vertical profiles of heating rate caused by aerosol light absorption are shown for aircraft observation days of 30 March, 2009 (14.17JST) and 05 April, 2009(14.67 JST). Figure 1 shows that some aerosol layers within an altitude of 2-6 km have strong heating rates comparable to the aerosols near the surface. For the aerosols that have relatively high heating rate, we noted that YSI and SSA values were relatively higher and lower, respectively (not shown here).This indicates that such strong heating rates over the boundary layer were likely to be caused by the mixture of dust and light absorbing aerosols. This result indicates that strongly light absorbing aerosols can be transported by dust aerosols at altitudes above the boundary layer in the spring season. Backward trajectories were used to trace the paths for aerosols on those layers. Backward trajectory analyses also emphasized that such light absorbing aerosol layers above the boundary layer were likely due to the mixture of aerosols transported from the desert and urban areas.

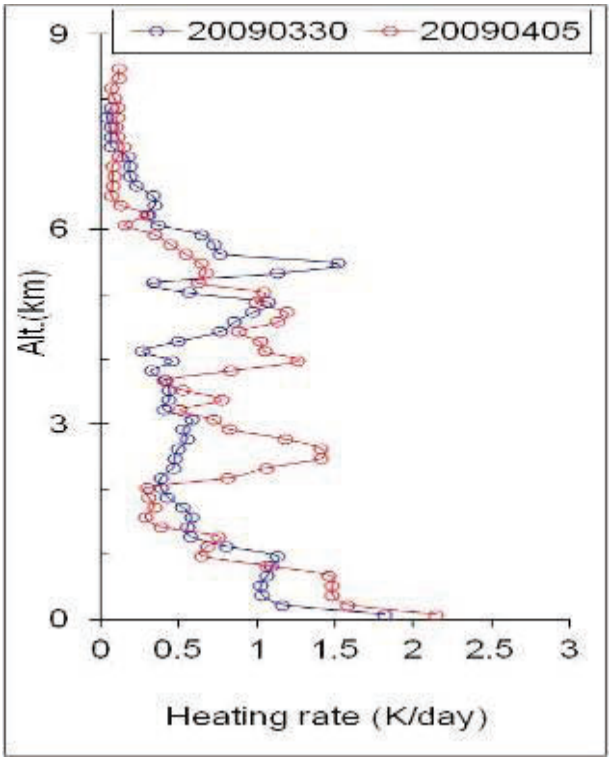

Figure 1 Vertical profiles of the heating rate due to aerosol absorption over Fukue-jima on 30 March 2009 (14.17 JST) and 05 April (14.67 JST) 2009. The vertical profiles were calculated from a combination of aircraft, lidar, and surface observation data.

1 Khatri, P., A. Yamazaki and Y. Kondo, 2012: Retrieval of key aerosol optical parameters from spectral direct and diffuse irradiances measured by a radiometer with nonideal cosine response characteristics, *J. Atmos. Oceanic Technol.*(in press)

2 Takamura, T., N. Sugimoto, A. Shimizu, A. Uchiyama, A. Yamazaki, K. Aoki, T. Nakajima, B. J. Sohn and H. Takenaka, 2007: Aerosol radiative characteristics at Gosan, Korea, during the Atmospheric Brown Cloud East Asian Regional Experiment 2005, *J. Geophys. Res.*,**112**, D22S36, doi: 10.1029/2007JD008506

3 Hess, M., P. Koepke and I. Schult, 1998: Optical Properties of Aerosols and Clouds: The software package OPAC, *Bull. Am. Met. Soc*., **79**, 831-844

4 Ricchiazzi, P., S. Yang, C. Gautier and D. Sowle, 1998: SBDART: A research and teaching software tool for plane-parallel radiative transfer in the Earth's atmosphere. *Bull. Amer. Meteor. Soc*., **79**, 2,101-2,114.

Particle effective density measurement using a DMA-APM-CPC system in Nagoya, Japan: Estimation of mixing state and shape

Tomoki Nakayama[1,*], Yuuki Sawada[1], Yuka Ikeda[1], Yutaka Matsumi[1], Yoshitaka Setoguchi[2], Kaori Kawana[2] and Michihiro Mochida[2]

[1]Solar-Terrestrial Environment Laboratory and Graduate School of Science, Nagoya University, Furo-cho, Chikusa-ku, Nagoya 464-8601, Japan
[2] Graduate School of Environmental Studies, Nagoya University, Furo-cho, Chikusa-ku, Nagoya 464-8601, Japan

Corresponding author. Tel.: +81 52 747 6413; Fax: +81 52 789 5787, Email address: nakayama@stelab.nagoya-u.ac.jp (T. Nakayama)

Simultaneous observations of particle density distributions and chemical properties of ambient aerosols were conducted at an urban site in Nagoya, Japan, during summer, by a system consisting of a differential mobility analyzer, an aerosol particle mass analyzer, and a condensation particle counter, and a time-of-flight aerosol mass spectrometer. Bimodal effective density distributions consisting of non-volatile black carbon particles and volatile compounds such as organics and sulfate were observed. Temporal variations of effective densities were found to be related to chemical composition. From the effective density distributions with and without heating, relative abundance of externally mixed soot particles was also estimated.

Keywords: Particle density distribution; Mixing state; Chemical property, Aerosol particle mass analyzer (APM); Time of flight aerosol mass spectrometer (ToF-AMS); Ambient measurement

1. Introduction

Tropospheric aerosols are a complex mixture, including mineral dust, inorganic salts, organic compounds, and soot particles. The climate impact of aerosols depends on their physical and chemical properties such as size, shape, density, mixing state, and chemical composition. Therefore, accurate knowledge of these properties is essential for modeling climate forcing by aerosols.

Particle density is an important parameter that links particle mass and particle volume (or diameter). However, detailed knowledge of the density distributions of ambient particles is still limited [e.g. 1-3], because filter-based techniques can provide only average densities of internally and externally mixed particles.

In this work, real-time measurements of effective density distributions and chemical properties of ambient particles were made at an urban site in Nagoya, Japan, and the relationship between them was examined. In addition, the mixing state of the aerosols, another important parameter for determining optical properties, was also estimated by using the measured particle density distributions.

2. Methods

Observations of aerosol density distributions and chemical properties were conducted on 16–25 August 2011 at the Higashiyama campus of Nagoya University. A schematic diagram of the experimental setup used for the ambient measurements is shown in Figure 1. The effective density of particles with mobility diameters of 100 and 200 nm was measured by a system consisting of a differential mobility analyzer (DMA, TSI model 3081), an aerosol particle mass analyzer (APM, Kanomax model 3601), and a condensation particle counter (CPC TSI, model 3776).

Nearly monodisperse aerosols were selected by the DMA, which was upstream of the APM. The APM then transmitted particles of known mass, determined by the balance of

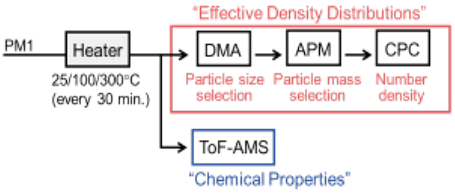

Figure 1 The experimental setup.

centrifugal and electrostatic forces, to the CPC, which was connected downstream of the APM and which counted the particles selected by the APM. By scanning the APM voltage with a fixed rotational velocity, the effective density distributions of the ambient particles were then determined [1].

Chemical compositions of the aerosol were measured by a time-of-flight aerosol mass spectrometer (ToF-AMS, Aerodyne). The density distributions and chemical compositions were measured after the aerosol had passed through a PM1 cyclone, diffusion dryers, and one of three heaters, controlled at 25, 100, and 300 °C, by switching ball valves every 30 min.

3. Results and discussion

The ambient aerosols typically had two distinct density peaks, at 0.7–0.9 g/cm^3 (peak 1) and 1.2–1.6 g/cm^3 (peak 2) (Figure 2). The changes in the peak areas after heating implied that peak 1 and peak 2 consisted mainly of soot and volatile compounds (such as inorganic salts and organics), respectively.

Observation data were divided into three periods on the basis of particle chemical properties and the observed meteorological conditions: A, 00:00 16 August to 06:00 20 August; B, 06:00 20 August to 12:00 22 August; and C 12:00 22 August to 06:00 25 August. These periods were characterized as follows: period A, increased mass concentration of organics and of the low-volatility oxygenated organic aerosol (LV-OOA) fraction during the afternoon (12:00–18:00) accompanied by clear weather conditions;

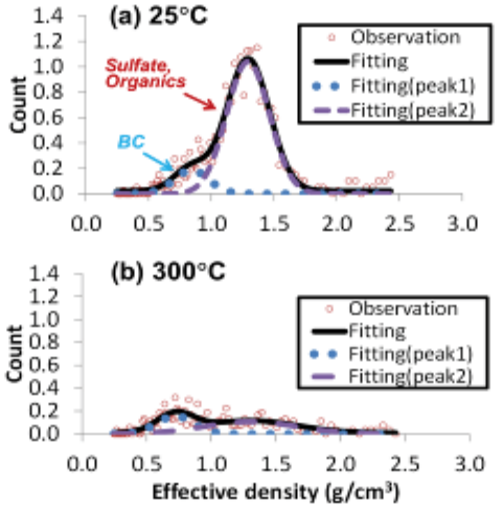

Figure 2 Average density distributions of ambient particles with a mobility diameter of 100 nm observed at an inlet temperature of (a) 25 °C and (b) 300 °C at 6:00–18:00 on 21 August 2011.

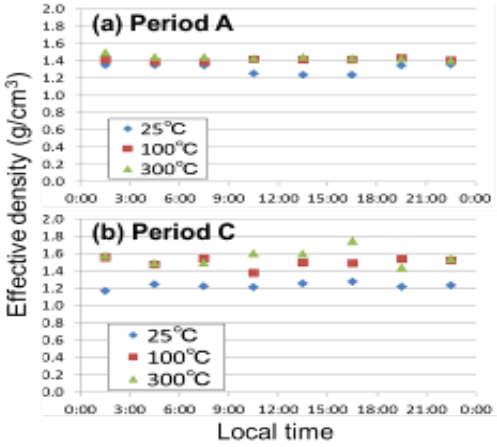

Figure 3 Diurnal variations of the average effective density of peak 2 during periods (a) A and (b) C (mobility diameter, 100 nm).

period B, lower abundance of volatile compounds (organics and inorganics) associated with rainfall; period C, higher sulfate/organics ratio (typically >2).

Analysis of the diurnal variation of the effective density of peak 2 during these periods (examples shown in Figure 3) showed that during period A, the effective density at 25 °C decreased during the afternoon (12:00–18:00), whereas no significant diurnal variations of effective density were observed at 100 °C or 300 °C. This result may be attributable to higher contributions of photochemically generated LV-OOA during the afternoon, because LV-OOA possibly has a relatively lower density. During period C, a larger difference in effective density was observed between 25 °C and 100 °C, which may be due to a higher contribution of sulfate during that period, because sulfate has a higher density and volatilization temperature than organics.

The peak area ratio of peak 1 to the sum of the areas of peak 1 and peak 2 gives information about the relative abundance of externally mixed black carbon (BC) particles. The ratio typically was between 0.05 and 0.15 at 25 °C for particles with a diameter of 100 as well as those with a diameter of 200 nm. The absolute peak area of peak 1 tended to increase after heating. This result implies that at 25 °C some of the BC particles were internally mixed with volatile compounds.

This work was partly supported by the Global Environment Research Fund of the Japanese Ministry of the Environment (RF-1008) and the Ministry of Education, Culture, Sports, Science and Technology (KAKENHI 20671001, 21710007, 22310015, 20120007).

1 McMarry, P. H., X. Wang, K. Park and K. Ehara, 2002: The relationship between mass and mobility for atmospheric particles: A new technique for measuring particle density, *Aerosol Sci Technol*. **36**: 227-238

2 Geller, M., S. Biswas and C. Sioutas, 2006: Determination of particle effective density in urban environments with a differential mobility analyzer and aerosol particle mass analyzer. *Aerosol Sci Technol*. **40**: 709-723

3 Spencer, M. T., L. G. Shields, K. Shields and A. Shields, 2007: Simultaneous measurement of the effective density and chemical composition of ambient aerosol particles. *Environ Sci Technol*. **41**, 1,303-1,309

Measurements of light absorption enhancement of black carbon using a photoacoustic spectrometer in Nagoya, Japan

Tomoki Nakayama[1,*], Yuka Ikeda[1], Yuuki Sawada[1], Yutaka Matsumi[1], Yoshitaka Setoguchi[2], Kaori Kawana[2] and Michihiro Mochida[2]

[1]Solar-Terrestrial Environment Laboratory and Graduate School of Science, Nagoya University, Furo-cho, Chikusa-ku, Nagoya 464-8601, Japan
[2]Graduate School of Environmental Studies, Nagoya University, Furo-cho, Chikusa-ku, Nagoya 464-8601, Japan

Corresponding author. Tel.: +81 52 747 6413; Fax: +81 52 789 5787, Email address: nakayama@stelab.nagoya-u.ac.jp (T. Nakayama)

Simultaneous observations of optical and chemical properties of ambient aerosols were conducted at an urban site in Nagoya, Japan, during summer by using a multi-wavelength photoacoustic spectrometer and a time-of-flight aerosol mass spectrometer. By comparing absorption coefficients at 781 nm with and without heating (300 °C), the increase in BC light absorption due to particle coating was estimated to be 10–40%. A slightly larger amplification factor was observed when the sulfate/organics ratio was high. The contribution to light absorption of organic carbon, which is vaporized at 300 °C, was small (<5%) at 405 nm, at least during the summer at Nagoya.

Keywords: Aerosol optical properties; Chemical properties; Absorption enhancement; Light absorbing organic carbon; Photoacoustic spectroscopy (PAS); Time-of-flight aerosol mass spectrometer (ToF-AMS); Ambient measurement

1. Introduction

Aerosol particles play an important role in the radiation balance in the atmosphere by absorbing and scattering incident light. Black carbon (BC) particles are an important global warming agent with radiation forcing similar in magnitude to that of CO_2. Light absorption by BC is generally considered to be increased by internal mixing with other compounds, but the amount of absorption enhancement depends on factors such as the refractive index of the BC and the coating materials and the size and location of the BC core. In addition, light-absorbing organic carbon ("brown carbon"), including humic-like substances (HULIS), organonitrates, and nitro-aromatics, has recently been proposed to be a cause of substantial absorption, particularly in the shorter visible and UV wavelengths. However, observational studies of the enhancement of BC light absorption and of brown carbon are still limited, mainly because it is difficult to directly measure light absorption by internally mixed BC particles without collecting them on a filter [1, 2].

In this work, photoacoustic spectroscopy was applied to examine light absorption enhancement of BC and the contribution of brown carbon to aerosol light absorption at an urban site in Nagoya, Japan.

2. Methods

Observations of aerosol optical and chemical properties were conducted during 16–25 August 2011 at the Higashiyama campus of Nagoya University. A schematic diagram of the experimental setup is shown in Figure 1. The optical properties and chemical compositions were measured after the aerosols were passed through a PM1 cyclone, diffusion dryers, and one of three heaters, controlled at 25, 100, and 300 °C, by switching ball valves every 30 min. Optical properties were measured using a photoacoustic soot spectrometer (PASS-3, Droplet Measurement Technologies). Chemical composition of the aerosol was measured by a time-of-flight aerosol mass spectrometer (ToF-AMS, Aerodyne). Mass concentrations of elemental carbon (EC) and organic carbon (OC) were also measured by a thermo-optical technique (Sunset Lab.) every 90 min.

3. Results and discussion

Observation data were divided into three periods on the basis of particle chemistry and meteorological conditions: A 23:00 15 August to 12:00 19 August; B, 12:00 19 August to12:00 22 August; and C, 12:00 22 August to 06:00 25 August. These periods were characterized as follows: period

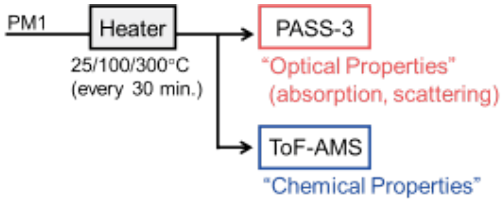

Figure 1 The experimental setup.

A, increased mass concentration of organics and of the low-volatility oxygenated organic aerosol fraction during the afternoon accompanied by clear weather conditions; period B, lower abundance of volatile compounds (organics and inorganics) associated with rainfall; and period C, higher sulfate/organics ratio (typically > 2), possibly due to long-range transport of sulfate.

Changes in the inlet temperature from 25 °C to 300 °C led to a slight decrease in the absorption coefficient ($b_{abs}(\lambda)$), but a significant decrease in the scattering coefficient ($b_{sca}(\lambda)$). As a result, small single scattering albedo (SSA; $b_{sca}(\lambda)/(b_{abs}(\lambda) + b_{sca}(\lambda))$) values of around 0.4 were observed at 300 °C (Figure 2). The ToF-AMS data showed that sulfate, nitrate, and a large part of the organics were volatized at the inlet temperature of 300 °C. These results suggest that the observed optical properties at 300 °C are mainly due to non-volatile BC particles.

Relatively smaller SSA values at 25 °C were observed during period B, when smaller mass concentrations of volatile compositions such as sulfate and organics were observed. These results may be explained by the hypothesis that lower photochemical activities due to a stationary front suppressed secondary formation of aerosols containing sulfate and organics, and resulted in larger contributions by light-absorbing BC particles during the period.

The amplification factor (F_A), which represents enhancement of light absorption by BC due to its coating, is calculated under the assumption that light absorption by OC is negligible at 781 nm as follows.

$$F_A = b_{abs}(781\ \text{nm}, 25\ °\text{C}) / b_{abs}(781\ \text{nm}, 300\ °\text{C}) \qquad (1)$$

Average F_A ($\pm 1\sigma$) (Figure 3a) during periods A, B, and C was 1.22 ± 0.16, 1.26 ± 0.14, and 1.29 ± 0.13, respectively. Although average F_A during period C, when the contributions of sulfate were large, was slightly higher than that during the other two periods, the small difference in F_A among the three periods suggests that the degree of enhancement of light absorption by BC due to its coating did not significantly depend on photochemical activities and aging processes in this observation.

The absorption coefficient of OC at 405 nm ($b_{abs,OC}$(405 nm, 25 °C)) was calculated under the assumption that F_A does not depend on wavelength as follows.

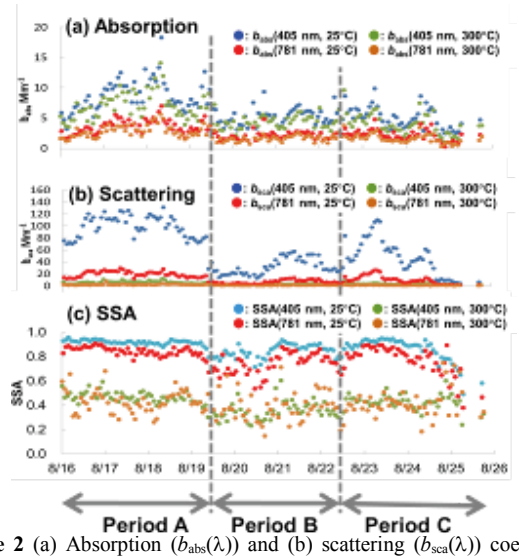

Figure 2 (a) Absorption ($b_{abs}(\lambda)$) and (b) scattering ($b_{sca}(\lambda)$) coefficients and (c) single scattering albedo (SSA; $b_{sca}(\lambda)/(b_{abs}(\lambda)+ b_{sca}(\lambda))$) at 405 and 781 nm measured at the inlet temperature of 25 °C and 300 °C. All data are 30-min averages.

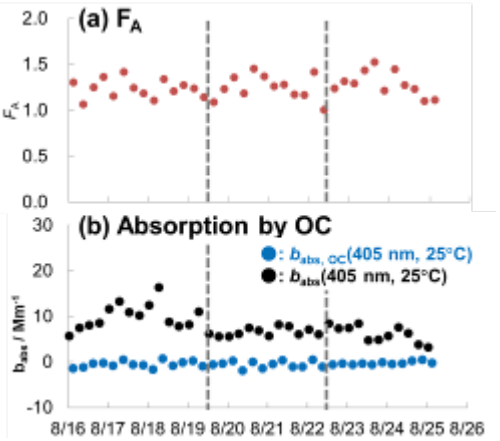

Figure 3 (a) Amplification factor (F_A) calculated with eq. (1) and (b) absorption coefficients for OC at 405 nm calculated with eq. (2) (see text). All data are 6-h averages.

$$b_{abs,OC}(405\ \text{nm}, 25\ °\text{C}) = b_{abs}(405\ \text{nm}, 25\ °\text{C}) - F_A \times b_{abs}(405\ \text{nm}, 300\ °\text{C}) \qquad (2)$$

The calculated $b_{abs,OC}$ values and the observed total aerosol light absorption at 405 nm show that the contribution of light absorption by OC, which is vaporized at 300 °C, was small (<5%) at 405 nm, at least during summer at Nagoya (Figure 3b).

This work was partly supported by the Global Environment Research Fund of the Japanese Ministry of the Environment (RF-1008) and the Ministry of Education, Culture, Sports, Science and Technology (KAKENHI 20671001, 21710007, 22310015, 20120007).

1 Flowers, B. A., M. K. Dubey, C. Mazzoleni, et al. 2010: Optical-chemical-microphysical relationships and closure studies for mixed carbonaceous aerosols observed at Jeju Island; 3-laser Photoacoustic spectrometer, particle sizing, and filter analysis, *Atmos Chem Phys*. **10**, 10,387-10,398.
2 Lack, D. A., M. S. Richardson, D. Law, et al. 2012: Aircraft instrument for comprehensive characterization of aerosol optical properties, Part 2: Black and brown carbon absorption and absorption enhancement measured with photoacoustic spectroscopy, *Aerosol Sci Technol*. **46**, 555-568.

Changes in chemical compositions of sea-salt particles collected at Mt. Rokko, Kobe, Japan

Shohei Mukai[1,*] and Ken'ichi Ohkushi[1]

[1]The Graduate School of Human Development and Environment, Kobe University, 3-11 Tsurukabuto, Nada-ku, Kobe 657-8501, Japan

Corresponding author. Email address: mukaishohei76@gmail.com (S. Mukai)

We collected aerosol particles at the summit of Mt. Rokko, Kobe, Japan, at 15:00 JST every day for one month from 31 July to 1 September 2011, and analyzed a total of 21 aerosol samples with a transmission electron microscopy system equipped with an energy-dispersive X-ray analyzer. Various aerosol particles having different chemical compositions were identified. In particular, the chemical compositions of sea-salt particles differed from that of typical seawater. We focused on four sea-salt particles from two samples. The amount of Cl varied with the sampling day, and the Na to Mg ratio in sea-salt particles differed from that of seawater.

Keywords: Aerosol particles; Sea-salt particles; Elemental composition; Single particle analysis; Electron microscopy; Chemical compositions; Electron micrograph

1. Introduction

Kobe city, including Mt. Rokko, is located in the northwestern part of the Kansai urban region, the second-most populated urban area in Japan. Kansai is also an active industrial region, where many studies of aerosol particles have been carried out. For example, Adachi (2006: Ref. 1) analyzed dry deposition of particles in winter and Iwasaki et al. (2007: Ref. 2) analyzed morphologies and chemical compositions of aerosol particles during Asian and non-Asian dust-storm events. Both these studies used scanning electron microscopy along with energy-dispersive X-ray analysis (SEM-EDX). Furthermore, Aikawa et al. (2003: Ref. 3) showed by a bulk analysis that aerosol particles were present during fog events at Mt. Rokko. Despite the many studies conducted in this region, single aerosol particles in summer have not been analyzed, even though single-particle analyses are an important method for obtaining basic information about the morphology and chemical composition of aerosol particles. The purpose of this study was to investigate the basic characteristics of aerosol particles sampled on Mt. Rokko in summer. Here we examine individual sea-salt particles obtained on Mt. Rokko in summer 2011 by transmission electron microscopy (TEM)-EDX.

2. Methods

Aerosol samples were collected at the summit of Mt. Rokko (34°77′N, 130°20′E, 931 m above sea level), Kobe, Japan (Figure 1), daily from 31 July to 1 September 2011 (except on 17, 25, 27, and 28 August). Aerosol samples were collected by a cascade impactor (model I-1L, PIXI International Corp.) with two stages having aerodynamic 50% cut off diameter of 1.0 and 8.0 μm. We used particles collected on the 1.0-μm-diameter stage. Samples were collected for 5 minutes beginning at 15:00 JST on each day.

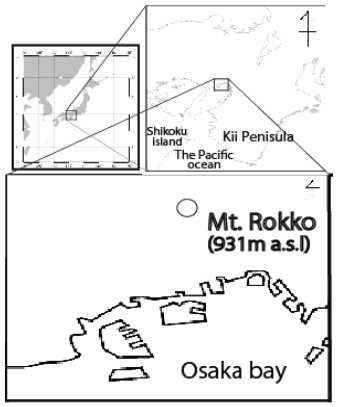

Figure 1 Location of the sampling site.

We chose two samples, one collected on 7 August and the other on 1 September, for analysis. Electron micrographs of aerosol particles were obtained by TEM (JEM-2010, JEOL Ltd.), and their chemical compositions were determined by EDS analysis (JED-2300T, JEOL Ltd.), conducted using an acceleration voltage of 200 kV and an EDX collection time of 30 s.

3. Results and discussion

Several hundred aerosol particles were captured on each grid on each of the two days, and many of them were sea-salt particles. We focused on four sea-salt particles and examined their features on electron micrographs (Figure 2) and ternary diagrams of their Na, S, and Cl contents (Figure 3).

On the ternary diagram, we also plotted the compositions of standard seawater and $NaNO_3$ and Na_2SO_4, which were generated by reacting sea-salt particles with HNO_3 and H_2SO_4, respectively, until they were completed depleted in Cl. Particles (a), (b), and (c) showed strong Cl depletion, but the Na/Cl ratio of particle (d) was similar to that of pure seawater (Figure 3). Thus, although these samples were collected at the same location and their morphologies were similar (Figure 2), their compositions differed greatly.

Many studies have investigated the modification of sea-salt particles in aerosols. For example, Li et al. (2003: Ref. 4) examined sea-salt particles collected over the North Atlantic and suggested that Cl modification occurred by chemical reactions with anthropogenic compounds such as sulfate and nitrate, and Kawakami et al. (2008: Ref. 5) suggested that the degree of modification depends on wind speed. An industrial area with a high population is situated south of our sampling site. The compositional differences among these samples may therefore reflect differences in the transport route and wind speed.

We also compared the relationship between Na and Mg in the four particles with that in seawater (Figure 4). The Na/Mg ratios of particles (b), (c), and (d) differed from the seawater ratio, whereas the ratio in particle (a) was almost the same as the seawater ratio. Thus, although Na/Cl in particle (d) was the same as that of seawater (Figure 3), its Na/Mg ratio differed. The particles of both samples were representative of aerosol particles collected at Mt. Rokko, where a wide range of Na and Mg contents is observed, possibly reflecting the influence of anthropogenic materials. Future studies are needed to understand urban atmospheric chemical processes over Kansai.

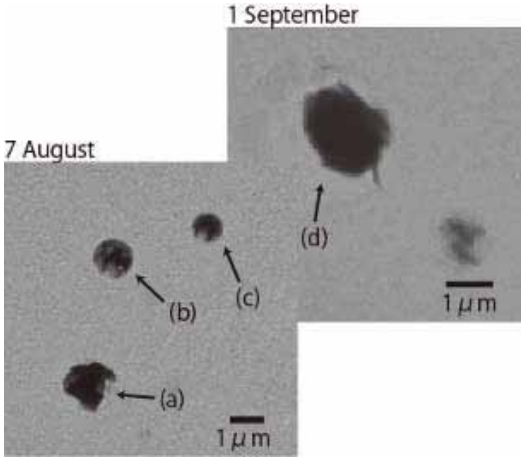

Figure 2 Photomicrographs of sea-salt particles collected on 7 August and 1 September..

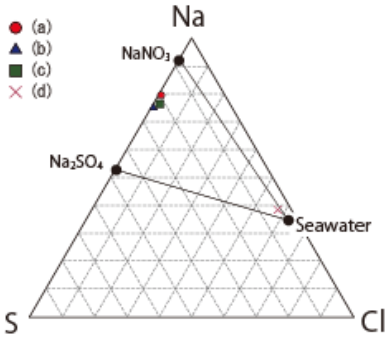

Figure 3 Ternary diagram of Na, S, and Cl. Na_2SO_4 and $NaNO_3$ were generated by reacting sea-salt particles with H_2SO_4 and HNO_3, respectively. See Figure 2 for the micrographs of particles (a), (b), (c), and (d).

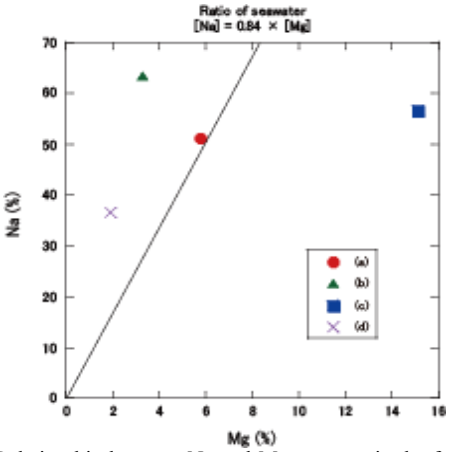

Figure 4 Relationship between Na and Mg contents in the four particles. The line on the graph shows the seawater ratio.

We thank K. Adachi (MRI), T. Hiraki (Hyogo Pref.), Y. Terakado, M. Iwasaki (Kobe Univ.), and K. Osada (Nagoya Univ.) for their help and support.

1 Adachi, K., 2006: Characterization of atmospheric dry deposition in Kobe, *Japan, Chemosphere*, **64**, 1,311-1,317.

2 Iwasaki, M., Y. Yagi and Y. Tainosho, 2007: Single particle analysis of atmospheric particulate matters collected in Kobe city at April and September, *J. Jap. Soc. Atmos. Environ*. **42**, 200-207 (in Japanese).

3 Aikawa, M., Hiraki, T., & Tamaki, M. (2006) Comparative field study on precipitation, throughfall, stemflow, fog water, and atmospheric aerosol and gases at urban and rural sites in Japan. *Science of the Total Environment,* **366**(1), 275-85. doi: 10.1016/j.scitotenv.2005.06.027.

4 Li, J., J. R. Anderson and P. R. Buseck, 2003: TEM study of aerosol particles from clean and polluted marine boundary layers over the North Atlantic. *Journal of Geophysical Research*, **108**(D6). doi: 10.1029/2002JD002106.

5 Kawakami, N., K. Osada, C. Nishita, M. Yabuki, H. Kobayashi, K. Hara and M. Shiobara, 2008: Factors controlling sea salt modification and dry deposition of nonsea-salt components to the ocean. *Journal of Geophysical Research*. **113**(D14), 1-13. doi:10.1029/2007JD

Laser post-ionization mass spectrometry of PAHs on diesel soot particles

Kenji Ohishi[1], Norihito Mayama[1,2], Kana Kitatsugu[2], Kentaro Misawa[2], Tetsuo Sakamoto[1] and Masaaki Fujii[2]

[1]Department of Electrical Engineering, Kogakuin University, 2665-1, Nakano-cho, Hachioji-City, Tokyo 192-0015, Japan
[2]Chemical Resources Laboratory, Tokyo Institute of Technology, 4259 Nagatsuta-cho, Midori-ku, Yokohama 226-8503, Japan

**Corresponding author. Tel.: & Fax: +81 42 628 4872; Email address: kt13222@ns.kogakuin.ac.jp (K. Ohishi)*

Polycyclic aromatic hydrocarbons (PAHs), which are found in diesel soot and suspended particulate matter, are well known to be harmful to human health. Pi-conjugated organic materials such as PAHs absorb photons in the ultraviolet light range. Here, we detected PAHs on diesel soot particles, chosen as suitable real environmental samples to demonstrate single-particle analysis by gallium focused ion beam time-of-flight secondary ion mass spectrometry (Ga-FIB-TOF-SIMS) and laser systems, including laser post-ionization sputtered neutral mass spectrometry. We optimized the Ga-FIB-TOF-SIMS apparatus to keep the sample at a low temperature of about 170 K to suppress the evaporation of PAHs from the sample, and for the laser post-ionization mass spectrometry, the apparatus incorporated a new optical system that allowed the focus to be adjusted by moving the laser and the lens in parallel in order for laser light to be accessible to the nearer point sputtered by FIB.

Keywords: Laser-SNMS; REMPI; Diesel soot; SPM; PAHs; Asian dust; Kosa; Single particle analyzer;

1. Introduction

Several kinds of polycyclic aromatic hydrocarbons (PAHs) are found on diesel soot particles, Asian dust "*Kosa*", and suspended particulate matter that are transported long distances. Because PAHs are well known to be harmful to human health, it is important to understand the long-range transport of Asian dust to study the internal and external mixing states of individual particles with inorganic and/or organic materials.

Our single-particle analyzer [1, 2] uses gallium focused ion beam time-of-flight secondary ion mass spectrometry (Ga-FIB-TOF-SIMS) and several laser systems. The combination of laser-induced resonance-enhanced multi-photon ionization (REMPI), laser post-ionization sputtered neutral mass spectrometry (laser-SNMS), and TOF mass spectrometry allows several highly selective and sensitive analytical techniques to be applied. To increase the sensitivity and selectivity of the analysis, sputtered neutral particles are post-ionized by irradiating them with an electron beam or photon field. Many experiments have been carried out with this system on inorganic and organic materials [3-7].

For REMPI and laser-SNMS experiments, the laser focus position, shape, and input energy are important for ionizing and detecting the materials with high sensitivity. In general, laser light is focused by a cylindrical or positive lens, but to move the focus point parallel in both vertical and horizontal directions along the optical beam axis, a system with a new type of focus lens and a movable light axis is needed to control the focus position.

In this paper, we report on optimizations of our apparatus for detection of PAHs, and we show an example of its use for detection of PAHs on diesel soot.

2. Experiment

Figure 1 shows our single-particle analyzer, which consists of a Ga-FIB-TOF-SIMS apparatus and laser systems, including a laser-SNMS system. To optimize the apparatus and suppress the evaporation of PAHs from the diesel soot sample, we modified the system so that it would keep the sample cool at about –100 °C (~170 K) by lowering the pressure in the chamber from atmospheric pressure to ultra-high vacuum pressure.

For laser post-ionization mass spectrometry, the handling of the laser light is very important. Many similar apparatuses have a simple positive lens or a cylindrical lens for focusing the laser light on the sample stage. We designed a new optical system that enabled us to move the focus point of the laser and the lens in parallel (Figure 2). We selected

laser light with a wavelength of 266 nm, and used a 266-nm pulsed laser beam timed to coincide with the FIB. Because PAHs have a pi-conjugated system, most PAH molecules are ionized by 1-color 2-photon process after they are sputtered by the FIB and have absorbed at least two photons during their exposure to the 266 nm laser light. As a result, it is possible to analyze PAHs by TOF-MS. In this study, we analyzed diesel soot particles by laser-SNMS.

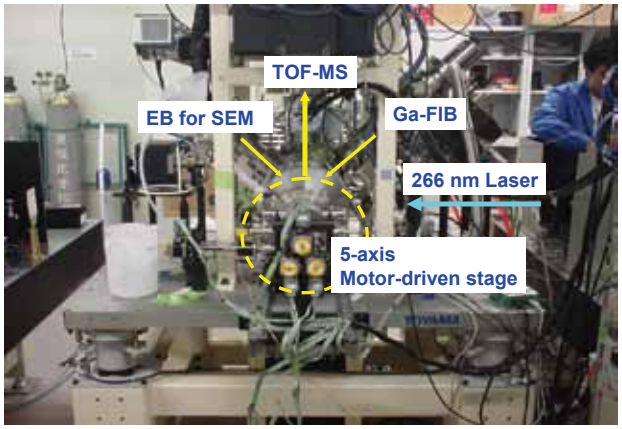

Figure 1 Instruments of time-of-fight secondary ion mass spectrometry and YAG + dye laser system. Repetition rate 30 Hz, pulse energy ~5mJ. TOF-MS: time-of-flight mass spectrometer, EB for SEM: electro beam for scanning electron microscope, Ga-FIB: gallium focused ion beam.

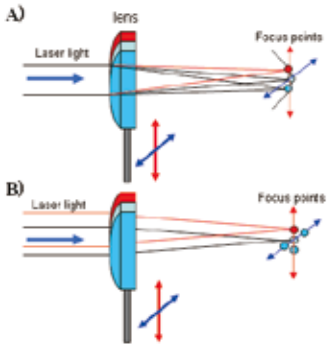

Figure 2 (Left): Diesel soot on the indium plate. The diesel soot was pressed on the flat indium plate and set in the sample stage. The sample was cooled below 170 K in the load lock chamber using liquid nitrogen. (Right): A) Old type focus shifter. The optical beam axis is fixed, and only the lens is moved. Therefore, in changing the focus horizontally and vertically, old type focus shifter moves the focal point to back and forth. B) New optical parallel axis and focus shifter. In front of the lens, the laser beam can be moved parallelly, horizontally and vertically. Also, the lens on the motor stage is simultaneously moved parallel to the laser. So this shifter keeps focal point no swingable back and forth for the area sputtered by FIB.

We chose diesel soot particles as a suitable real environmental sample to use as an example. The sample was collected from a diesel bus exhaust pipe with a diesel particulate filter (DPF). Several milligrams of diesel soot particles were pressed onto an indium metal substrate.

In the case of non-conductive materials, such as diesel soot, charge-up is caused by bombardment of the Ga-FIB; therefore, a low-energy electron gun for charge neutralization was also used to compensate for the charge-up. In addition, PAHs have a vapor pressure of several kilopascals (kPa). Injection of the PAH sample into the system at room temperature would cause the PAHs to evaporate from the sample. Therefore, to suppress the evaporation of PAHs, the sample was cooled by using liquid nitrogen under ultra-high vacuum pressure.

3. Results and discussion

Laser-SNMS analysis performed with the apparatus modified to incorporate a sample cooling system and an optical parallel axis and focus shifter successfully detected PAHs on diesel soot (Figure 3). The mass-to-charge (*m/z*) ratios of PAHs with 3 or 4 rings were detected, but not those of PAHs with 5 or more rings.

In previous other experiments, pyrene and benzopyrene were found to coexist in diesel soot, but the molar ratios of pyrene and benzopyrene drastically changed at the different emission patterns [8]. Our result shows that benzopyrene quite probably was caught in the DPF or the emission pattern of diesel engine was very low. We did not identify benzopyrene on laser-SNMS spectra obtained by several analyses of diesel exhaust soot.

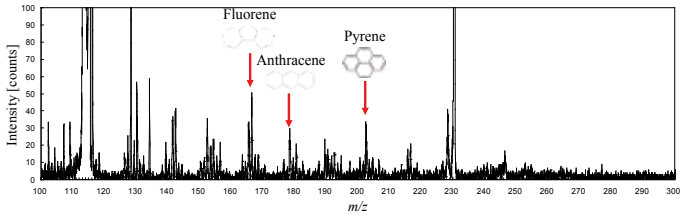

Figure 3 Laser post ionization mass spectrum of PAHs on diesel soot. The results suggest the mass-to-charge ratio values (*m/z*) is several PAHs detected in diesel soot by laser post-ionization mass spectrometry.

This research was supported by the Environment Research and Technology Development Fund (number B-1006), Ministry of the Environment, Japan.

1 Sakamoto, T., et al. 2008: *Applied Surface Science*, **255**(4), 1,617-1,620.
2 Koizumi, M., et al. 2008 : *Applied Surface Science*. **255**(4), 901-904
3 Wucher, A., J.C. Vickerman and D. Briggs (Eds.), 2001: ToF-SIMS: Surface Analysis by Mass Spectrometry, *IM Publications,* p .347.
4 Mazarov, P., A.V. Samartsev and A. Wucher, 2006: *Appl. Surf. Sci*. **252**, 6,452.
5 King, B.V., J.F. Moore, W.F. Calaway, I.V. Veryovkin and M.J. Pellin, 2006: *Appl. Surf. Sci*. **252**, 6,426.
6 Peterson, R.E., et al. 2006 : *Appl. Surf. Sci*. **252**, 7006.
7 Samartsev A.V. and A. Wucher, 2006: *Appl. Surf.* Sci. **252**, 6470.
8 Ji Yi Lee, et al. 2006 : *J. Geophys. Res.* **111**, D11303.

Analysis of black carbon particles by high-resolution TOF-SIMS

Norihito Mayama[1, 2,*], Yusuke Miura[2], Kenji Ohishi[2], Tetsuo Sakamoto[2] and Masaaki Fujii[1]

[1]Chemical Resources Laboratory, Tokyo Institute of Technology, 4259 Nagatsuta-cho, Midori-ku, Yokohama, Kanagawa 226-8503, Japan
[2]Department of Electrical Engineering, Kougakuin University, 2665-1 Nakano-machi, Hachioji, Tokyo 192-0015, Japan

Corresponding author. Tel.: +81 42 628 4872, Email address: mayama.n.aa@m.titech.ac.jp (N. Mayama)

We analyzed particles containing black carbon by time-of-flight secondary ion mass spectrometry with a high lateral resolution. After sulfate particles with a diameter of about 1 μm were sputtered by gallium primary ions (a gallium focused ion beam), solid materials with a diameter of about 100 nm were sometimes found within the particles. Since the mass spectrum for the solid material was almost the same as that of graphite, we concluded that the solids might be black carbon. Furthermore, we inferred a possible structure from the results, in which black carbon occurred at one edge of sulfates, and the sulfates were usually surrounded by organic matter.

Keywords: Black carbon; Aerosol particles; Time-of-flight secondary ion mass spectrometer; Single-particle analysis; Focused ion beam; Mass spectrum

1. Introduction

Black carbon, which is emitted by incomplete combustion of fossil fuel, biofuel, and biomass carbon, is a major contributor to global warming because in the air it absorbs solar radiation. Aerosol particles containing black carbon are typically aggregated carbonaceous spherules a few tens of nanometers in diameter that are coated with sulfates and/or organic matter. It is important to know the structure and composition of these particles for use in climate simulations [1]. Because of the small size of black carbon, transmission electron microscopy (TEM), electron energy-loss spectroscopy (TEM-EELS), and energy dispersive X-ray spectroscopy (EDX) [2] are most often used for their analysis. However, the structures of aerosol particles containing black carbon and the composition of the coating materials have yet to be clarified.

We developed a time-of-flight secondary ion mass spectroscopy (TOF-SIMS) system with high lateral resolution [3]. The apparatus can analyze single aerosol particles with the high lateral resolution of 40 nm, and a cross-section of the particle can be fabricated by using a gallium focused ion beam (FIB). Individual aerosol particles have already been analyzed with the apparatus to clarify their chemical reactions and sources [4, 5]. In this study, we used the apparatus to analyze aerosol particles containing black carbon.

2. Methods

Aerosol particles were collected at the Fukue-Jima Island, Nagasaki Prefecture, Japan, and on the Kougakuin University campus (Hachioji, Tokyo, Japan). A custom-made single stage impactor [6] was used for the sampling. The impactor collected particles less than 10 μm in diameter. Silicon wafers with an area of 4 mm^2 were used as collection substrates. Each sampling was performed for 10 minutes at a suction rate of 1.5 L/min. The silicon wafers with aerosols were introduced into the TOF-SIMS apparatus at room temperature and without any pretreatment.

All experiments described here were performed with a TOF-SIMS apparatus developed by the authors [3]. The apparatus has two beams: a gallium FIB as the primary ion beam and an electron beam (EB). The FIB was used as a machining tool to fabricate particles, to observe the particle surface, and to map the elements of the particle. A 30-keV gallium FIB was rastered to obtain the FIB-induced secondary electron image. The EB was used to search for particles to be analyzed and observe during the FIB machining. The base pressure of the apparatus was around 3.0×10^{-6} Pa.

First, aerosol particles on the silicon wafer were observed on the FIB-induced secondary electron image and the secondary electron image produced by the EB. Next, elemental mapping was performed using a pulsed FIB and TOF mass

spectrometry (MS) of an area a few tens of square micrometers in size on the silicon wafer, involving particles with a diameter of about 1 μm (128 × 128 pixels). The pulse duration was 300 ns, and 300 sweeps were performed. The FIB current was about 300 pA.

3. Results and discussion

Figure 1 shows the FIB-induced secondary electron image of a particle with a diameter of about 1 μm after ion sputtering. A solid material with a diameter of about 100 nm remained at the edge of the particles. The solid was not spherical but irregular in shape, similar to aggregated carbonaceous spherules observed by TEM [2]. This solid might be composed of black carbon.

Elemental mapping in negative analysis mode of particles with a diameter of about 1 μm before the sputtering showed an area of sulfate ions surrounded by carbon ions. In contrast, after the sputtering, an area of carbon ions was observed at one edge of the sulfates, which is consistent with the position of the solid material seen in Figure 1. However, the elemental mapping alone could not identify the carbon ions after the ion sputtering as black carbon, because the source of the carbon before and after ion sputtering was not clear.

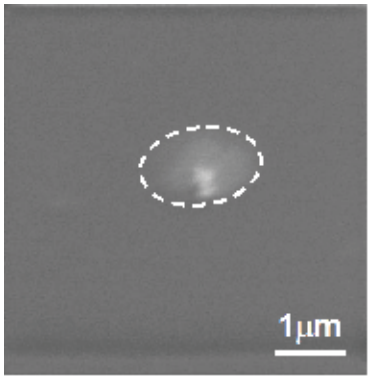

Figure 1 FIB-induced secondary electron image of particles with a diameter of about 1 μm after ion sputtering.

In the mass spectrum of the carbon area after ion sputtering (Figure 2), the carbon cluster ions C^-, C_2^-, C_3^-, C_4^-, C_5^-, and C_6^- were detected. In particular, C_3^- and C_6^- (m/z = 36 and 72, respectively) could be distinguished. The line at m/z = 48 is interpreted as C_4^- rather than SO^- because SO_2^- (m/z = 64) was not detected. The detected ions in the carbon area after ion sputtering were almost the same as those of graphite, used as a reference for elemental carbon. In addition, the solid carbon material remaining after ion sputtering was identified as black carbon. The materials in the carbon area

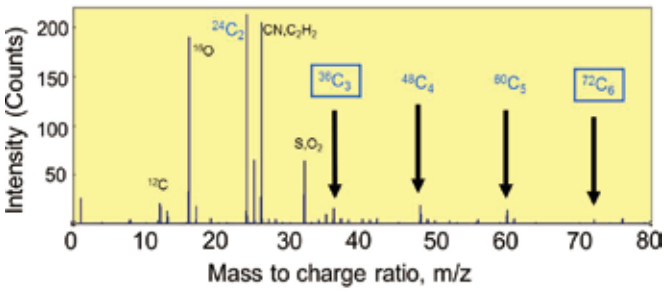

Figure 2 Mass spectrum of the carbon area of particles with a diameter of about 1 μm after ion sputtering

before ion sputtering were identified as organic matter from their mass spectra.

These results suggest that in the structure of the original aerosol particles containing black carbon. The black carbon may have been at one edge of the sulfates, and that the sulfates were usually surrounded by organic matter.

4. Summary

Aerosol particles containing black carbon were analyzed with a high lateral resolution TOF-SIMS system. After sulfate particles with a diameter of about 1 μm were sputtered by FIB, solid materials sometimes remained in the particles. On the basis of our analysis results, we concluded that the solids might be identified as black carbon. Furthermore, the aerosol particles containing black carbon might have a structure in which the black carbon is at one edge of sulfates, and the sulfates are usually surrounded by organic matter.

This work was supported by the Environment Research and Technology Development Fund (ERTDF, Ministry of the Environment, Japan, B-1006).

1 Moteki, N. and Y. Kondo 2007: Effects of mixing state on black carbon measurement by laser-induced incandescence. *Aerosol Science and Technology*, **41**: 398–417

2 Adachi, K., S. H. Chung and P. R. Buseck, 2010: Shapes of soot aerosol particles and implications for their effects on climate. *Journal of Geophysical Research*, **115**: doi: 10.1029/2009JD012868

3 Sakamoto, T., M. Koizumi, J. Kawasaki, et al. 2008: Development of a High Lateral Resolution TOF-SIMS Apparatus for Single Particle Analysis. *Applied Surface Science*, **255** (4): 1,617-1,620

4 Sakamoto, T., A. Takami, S. Hatakeyama, et al. 2012: Individual Analysis of Atmospheric Aerosol Particles at West-Japan Area using High Lateral Resolution Time-of-Flight Secondary Ion Mass Spectrometry. *Abstract of International symposium on aerosol studies explored by electron microscopy*. p.29

5 Mayama, N., E. Goto, Y. Miura, et al. 2012: Development of Source Apportionment of Individual Particle by High Resolution Time of Flight- Secondary Ion Mass Spectrometry. *Journal of the Vacuum Society Japan*, **55** (3): 104-107

6 Yamaguchi, J. and T. Sakamoto, 2008: A Portable Aerosol Sampler for Individual Particle Analysis by Means of TOF-SIMS. *Applied Surface Science*. **255** (4): 1,505-1,508

Analysis of source apportionment and chemical transformation of particles in trans-boundary air pollution using high lateral resolution imaging SIMS

*Tetsuo Sakamoto[1], Kenji Ohishi[1], Yusuke Miura[1], Masaaki Fujii[2], Kentaro Misawa[2], Norihito Mayama[2], Mikko Riese[2], Kana Kitatsugu[2], Akinori Takami[3], Satoshi Irei[3], Shiro Hatakeyama[4], Ayako Yoshino[4], Kentaro Murano[5], Takuma Mukaida[5], Hiroshi Bandow[6] and Yasuhiro Sadanaga[6]

[1]Department of Electrical Engineering, Faculty of Engineering, Kogakuin University, 2665-1 Nakano-machi, Hachioji, Tokyo 192-0015, Japan
[2]Chemical Resources Laboratory, Tokyo Institute of Technology, 4259 Nagatsutacho, Midori-ku, Yokohama, Kanagawa 226-8503, Japan
[3]Asian Environment Research Group, National Institute for Environmental Studies, 16-2 Onogawa, Tsukuba, Ibaraki 305-8506, Japan
[4]Graduate School of Agriculture, Tokyo University of Agriculture and Technology, 3-8-1 Harumicho, Fuchu, Tokyo 183-8538, Japan
[5]Department of Chemical Science and Technology, Faculty of Bioscience and Applied Chemistry, Hosei University, 3-7-2 Kajino-cho, Koganei-shi, Tokyo 184-8584, Japan
[6]Department of Applied Chemistry, Graduate School of Engineering, Osaka Prefecture University, 1-1 Gakuen-cho, Naka-ku, Sakai, Osaka 599-8531, Japan

Corresponding author. Tel.: +81 42 628 4872; Fax: +81 42 628 4872, Email address: ct13087@ns.kogakuin.ac.jp (T. Sakamoto)

Aerosol particles collected on the Fukue-Jima Island in western Japan were analyzed individually by a time-of-flight secondary ion mass spectrometry (TOF-SIUS) system with high lateral resolution. Two major coarse particle types were found in the sample from an air mass that had passed over the Korean Peninsula: one with a crystalline part, and another with a fluidic part. Examination of the first type showed that formed by the reaction of mineral dust containing $CaCO_3$ with HCl that had been produced by a decomposition reaction between sea salt and dust. The latter reaction would be enhanced in the presence of the pollutant HNO_3.

Keywords: Aerosol particles; Mixing properties of aerosols; Single particle analysis; TOF-SIMS

1. Introduction

Trans-boundary air pollution is of great interest because of its potential impacts on the environment in the downstream area. Aerosols transported from East Asia to western Japan have been studied to determine their sources and the chemical transformations that they undergo during transport. Conventionally, aerosol studies have employed chromatography and mass spectrometry to analyze particle composition. These analysis methods result in highly precise compositional data on bulk samples, but they cannot be used to analyze individual particles.

We formed a research group with the aim of combining bulk analysis with individual particle analysis. Bulk analysis was used to obtain information about overall trends in aerosol transport, and then individual particles from particular samples identified as of interest by the bulk analysis were analyzed. For individual particle analysis, a novel imaging apparatus based on time-of-flight secondary ion mass spectrometry (TOF-SIMS) was employed [1]. Here, we present the results of some individual aerosol particle analyses.

2. Methods

Aerosol particles were collected at the Fukue-Jima Island, Nagasaki prefecture, Japan, at 16:50 JST on 29 March and at 9:30 on 31, March 2010. A custom-made single-stage impactor [2] was used for the sampling. Silicon wafers 4×4 mm in size were used as collection substrates because it is easy to observe small particles on them owing to their surface smoothness. Each sampling was performed for 10 min at a pumping rate of 1.5 L/min. After the sampling, the wafers were stored in airtight boxes at room temperature

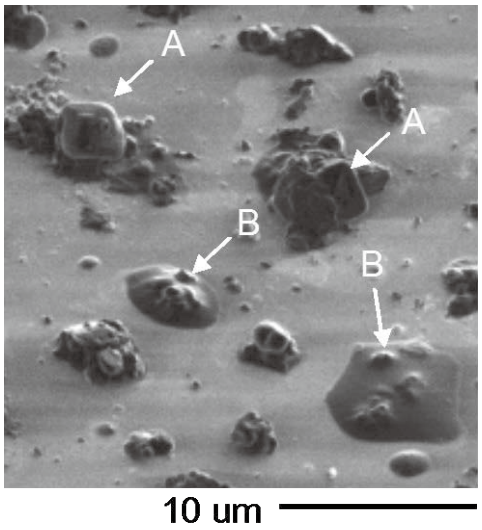

Figure 1 FIB-induced secondary electron image of aerosols collected on a Si wafer on 29 March. Particle type A is partly crystalline, and particle type B is partly fluidic.

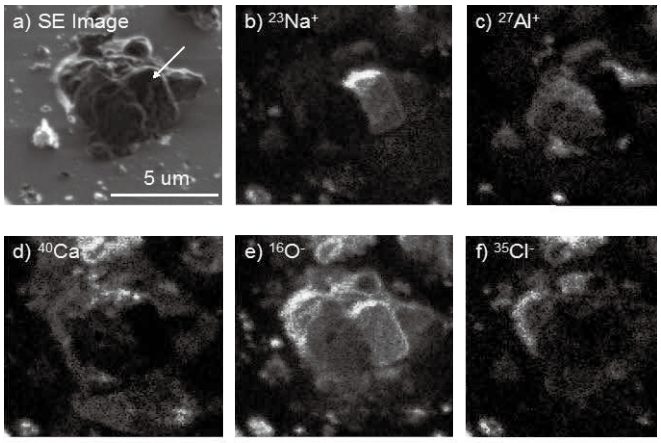

Figure 2 Secondary electron (SE) image (a) and secondary ion maps of a type A particle: (b) $^{23}Na^+$; (c) $^{27}Al^+$; (d) $^{40}Ca^+$; (e) $^{16}O^-$; (f) $^{35}Cl^-$. The arrow in (a) indicates the crystalline part.

until analysis in the laboratory.

All analyses were performed with a high-resolution TOF-SIMS apparatus. This apparatus can perform single-particle analysis with high lateral resolution, down to 40 nm. A cross section of the targeted particle is fabricated with a gallium focused ion beam (Ga-FIB) operated in DC mode at 30 keV, with a beam current of 300 to 500 pA and at an incident angle of 45° with respect to the surface normal. The Si wafers with the collected aerosols were introduced into the apparatus at room temperature and without any pretreatment. The particles were mapped at a resolution of 128 pixels × 128 pixels with a Ga-FIB pulse repetition of 200 per pixel. The typical time required for one mapping analysis was 300 s. The pressure in the specimen chamber was around 3.0×10^{-6} Pa.

3. Results and discussion

Before the individual particle analysis, the origin of each day's air mass was deduced by back-trajectory analysis using the HYSPLIT-4 method of the U.S. National Oceanic and Atmospheric Administration [3]. The air mass sampled on 29 March had passed over the Korean Peninsula, whereas that sampled on 31 March first passed over the Japanese Islands and then subsequently moved northward into the Pacific Ocean. Therefore, we expected that the particles collected on 29 March would be more affected by anthropogenic chemical species than those collected on 31 March.

In the FIB-induced secondary electron image of particles collected on 29 March (Figure 1), two major types of coarse particles were observed: type A particles were partly crystalline, and type B particles were partly fluidic.

Secondary ion maps of the major constituents of a type A particle analyzed by SIMS (Figure 2) show that the particle consisted of a crystalline part surrounded by non-crystalline components. The crystalline part (arrow in Figure 2a) consisted of Na and O, not of Na and Cl (sea salt). If the Na originated from sea salt, then the following sea salt decomposition reaction must have occurred in the air mass:

$$NaCl + HNO_3 \rightarrow NaNO_3 + HCl. \qquad (1)$$

In this reaction, HNO_3 is assumed to be emitted from industrial processes. The non-crystalline parts of the particle contained Cl and the mineral dust components Al and Ca, indicating that mineral dust had reacted with the HCl produced by the decomposition reaction.

4. Conclusion

Trans-boundary aerosol particles were individually analyzed with a state-of-the-art SIMS apparatus. An air mass that had passed over the Korean Peninsula had two major types of particles. One type contained $CaCl_2$ that originated from a reaction between mineral dust and sea salt.

This work was supported by the Environment Research and Technology Development Fund (ERTDF, Ministry of the Environment, Japan, B-1006), which is greatly appreciated.

1 Sakamoto, T., M. Koizumi, J. Kawasaki and J. Yamaguchi, 2008: *Appl. Surf. Sci*., **255**, 1,617.
2 Yamaguchi, J. and T. Sakamoto, 2005 : *Appl. Surf. Sci*. **255** (4), 1,505.
3 http://ready.arl.noaa.gov/HYSPLIT.php

Mixing state of atmospheric black carbon particles and its effect on light absorption

Hiroaki Naoe[1,*] and Kikuo Okada[1]

[1] Atmospheric Environment and Applied Meteorology Research Department, Meteorological Research Institute, 1-1 Nagamine, Tsukuba, Ibaraki 305-0052, Japan
[2] Present affiliation: Ozone Layer Monitoring Office, Japan Meteorological Agency, 1-3-4 Otemachi, Chiyoda-ku, Tokyo 100-8122, Japan

Corresponding author. Tel.: +81 3 3212 8341(ext.4212); Fax: +81 3 3211 4640, Email address: hnaoe@met.kishou.go.jp (H. Naoe)

The mixing state of light-absorbing carbonaceous particles is investigated in relation to their light-absorption properties by electron microscopy examination, analyses of black carbon (BC) on a quartz fiber filter by the thermal/optical reflectance method, and measurements made with two continuous light-absorbing photometers at a suburban site in Tsukuba, about 60 km northeast of Tokyo, Japan. The volume fraction of water-soluble material (ε) in individual particles is an important parameter for assessing particulate light absorption and/or scattering by atmospheric aerosols. The ε values in BC particles are evaluated by examining electron micrographs before and after dialysis (extraction) of water-soluble material. In BC particles with radii between 0.05 and 0.5 μm, the mass absorption coefficient (in units of $m^2 g^{-1}$) tends to increase as the average ε value increases, indicating that coatings of water-soluble material around BC particles can enhance their absorption of solar radiation. Moreover, the single scattering albedo also increases because a large amount of coating material will scatter more light.

Keywords: Aerosol particles; Elemental composition; Mixing properties of aerosols; Single particle analysis; Electron microscopy

1. Introduction

Light-absorbing carbonaceous particulate matter, often called "black carbon" (BC) or "soot," is an important constituent of atmospheric particles. Airborne BC is the most important particulate material absorbing solar radiation in the atmosphere, and it is one of major contributors to global climate forcing (IPCC, 2007). A mass absorption coefficient (MAC; in units of $m^2 g^{-1}$), which is defined as the ratio of the aerosol absorption coefficient (m^{-1}) to the mass concentration ($\mu g\ m^{-3}$) of the absorbing particles, is a crucial parameter in many applications. For BC particles with known size distribution and refractive index, MAC can be calculated by using a Mie theory. BC-containing aerosol particles can have MAC values between 3.8 and 17 $m^2 g^{-1}$ [1] or between 5 and 13 $m^2 g^{-1}$ [2], depending on the size distribution and the refractive index.

Measurements of BC concentrations or model calculations often use values on the order of 10 $m^2 g^{-1}$. Hansen (2003: Ref. 1) showed when measurements of aerosol absorption by soot absorption photometer were regressed against Aethalometer measurements of mass concentration, the resulting regression line had a slope of 10.8 $m^2 g^{-1}$. However, Bond and Bergstrom (2006: Ref. 2) recommended a MAC value of 7.5 $m^2 g^{-1}$ at or near combustion sources. To evaluate the contribution of different substances to light absorption by BC-containing particles, the mixing state of BC with other particulate matter (usually non-light-absorbing substances) must be considered [3]. Externally mixed BC particles have a lower MAC than internally mixed particles with the same chemical composition [1, 4].

To date, our understanding of light absorption obtained from measurements is insufficient because there were only a few studies to evaluate light absorption properties in BC-containing aerosol particles in relation to their mixing state. Thus, the aim of this study is to obtain information on the mixing state of BC particles by using electron microscopy and to evaluate its effect on the light absorption properties of BC-containing particles determined from observational results obtained in the suburban atmosphere of Tsukuba, Japan.

2. Methods

Ground-based aerosol measurements were performed in

the radiation observation building of the Meteorological Research Institute (MRI, 36.06°N, 140.01°E) in Tsukuba in October 2005. Naoe et al. (2009: Ref. 6) described the observational method in detail. Number-size distributions of aerosol particles were measured with a differential mobility analyzer (TSI, Model 3071A) in combination with a condensation nucleus counter (TSI, Model 3025). Aerosol particles were collected on carbon-coated nitrocellulose film in an impactor with a 0.5-mm-diameter round jet. After the collection, the particles on the film are coated with a Pt/Pd alloy at a thickness of 0.7 nm and a shadowing angle of 26.6°. Then, the shape and volume of the individual particles are assessed by using transmission electron microscopy (Hitachi, H-600 and H-6010). The system for measuring their optical properties consists of an integrating nephelometer (TSI, Model 3563), a continuous light absorbing photometer (PSAP; Radiance Research, M903), and a seven-wavelength black carbon aethalometer (Magee Scientific Company, AE-31).

Before sampling, quartz fiber filters (47 mm in diameter) for total suspended particulates were used that were punched out of a filter sheet of the same lot. For concentrated filtration, the aerosol particles were collected in an 8-mm-diameter area on the filter using a mask. Organic carbon (OC) and elemental carbon (EC) are analyzed with a DRI model 2001 carbon analyzer [7]. The IMPROVE protocol uses for the analysis and comprises the following seven steps: OC1, 120 °C; OC2, 250 °C; OC3, 450 °C; and OC4, 550 °C in a 100% He atmosphere; EC1, 550 °C; EC2, 700 °C; and EC3, 800 °C in a 2% O_2 and 98% He atmosphere.

3. Results

Figure 1 shows the relationship between MAC and the average volume fraction of water-soluble material ε in BC particles ($0 \leq \varepsilon < 1$) with radii between 0.05 and 0.5 μm in each sample. MAC is the ratio of the aerosol absorption coefficient at 565 nm, obtained from the PSAP measurements, to the BC mass concentration, measured by the thermal/optical reflectance method. MAC thus does not depend on the total particulate mass but on the mass of the only BC component. Although MAC is a function of wavelength and its properties determined at a single wavelength are insufficient for climate modeling studies, here we focus on identifying BC optical properties at a mid-visible wavelength (565 nm). For the Tsukuba aerosol collected in October 2005, the MAC values are distributed within a narrow range (10–13 $m^2\ g^{-1}$), and MAC tends to increase as the average volume fraction of water-soluble material increases. MAC (y-axis) and average ε (x-axis) are somewhat correlated ($r^2 = 0.41$; regression line, $y = 4.5x + 11.1$ (± 1.0) $m^2\ g^{-1}$). Therefore, the enhancement of MAC in our observational results is qualitatively comparable to that obtained by theoretical calculations. Since BC is fully externally mixed when $x = 0$, MAC in BC particles without water-soluble components is shown by the y-intercept to be 11.1 ± 1.0 $m^2\ g^{-1}$. Thus, this value is different from the value of 7.5 for ε = 0.0 recommended by Bond and Bergstrom (2006: Ref. 2).

Bond and Bergstrom (2006: Ref. 2) showed that MAC of BC particles ranges usually between 5 and 13 $m^2\ g^{-1}$ but that at or near combustion sources it does 6.3–8.6 $m^2\ g^{-1}$. Although a MAC of 10 $m^2\ g^{-1}$ is commonly cited, they recommended a MAC of 7.5 ± 1.2 $m^2\ g^{-1}$ for uncoated (i.e., freshly produced) aerosols and small BC particles. Our MAC value estimated from the y-intercept of the regression line is similar to the commonly cited value.

When ε is close to 1, BC particles correspond to be fully internally mixed. The estimated MAC value of 16 ± 1 $m^2\ g^{-1}$ in our result may represent the maximum of MAC that can result from the coating of BC particles.

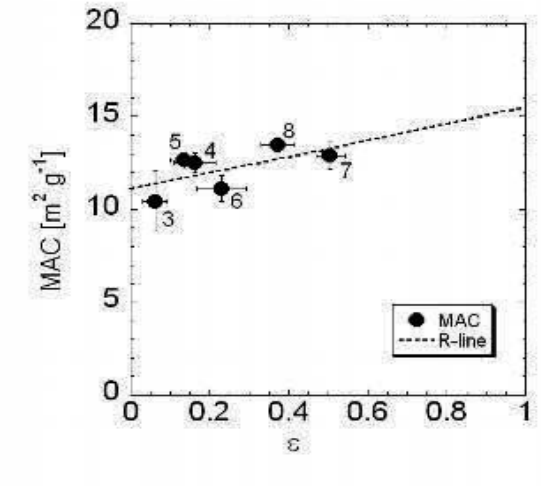

Figure 1 Mass absorption coefficient (MAC; aerosol absorption coefficient divided by BC mass concentration) versus the average volume fraction of water-soluble material (ε) in BC particles. BC mass concentrations were obtained by the thermal/optical reflectance method. The numbers close to the symbols indicate the sample IDs.

1 Horvath, H., 1993: Atmospheric light absorption - A review. *Atmos. Environ*. **27A**, 293-317.

2 Bond, T.C. and R.W. Bergstrom, 2006: Light absorption by carbonaceous particles: An investigative review. *Aerosol Sci. and Technol*. **40**, 27-67.

3 Naoe, H., and Okada K. 2001: Mixing properties of submicrometer aerosol particles in the urban atmosphere -with regard to soot particles, *Atmos. Environ*. **35**, 5765-5,772.

4 Heintzenberg, J., 1978: Light scattering parameters of internal and external mixtures of soot and non-absorbing material in atmospheric aerosols. *Proceedings of the Conference on Carbonaceous Particles in the Atmosphere*, Berkeley, CA. 278-281.

5 Hansen, A.D.A., 2003. The Aethalometer Manual. Berkeley, CA, USA: *Magee Scientific*.

6 Naoe, H., S. Hasegawa, J. Heintzenberg, K. Okada, A. Uchiyama, Y. Zaizen, E. Kobayashi and A. Yamazaki, 2009: State of mixture of atmospheric submicrometer black carbon particles and its effect on particulate light absorption. *Atmos. Environ.*, **43**, 1,296–1,301.

7 Hasegawa, S., S. Wakamatsu and K,Tanabe, 2005: Comparison of particulate carbon analysis between the thermal method and the thermal/optical method using the same ambient samples. *Journal of Japan Society for Atmospheric Environment* **40**, 181–192 (in Japanese).

Fine mineral aerosols collected in Japan during two Asian dust events: Size distributions and mixing properties

Yuji Zaizen[1]*, Hiroaki Naoe[1], Hiroshi Takahashi[1] and Kikuo Okada[1]

[1] Atmospheric Environment and Applied Meteorology Research Department, Meteorological Research Institute, 1-1 Nagamine, Tsukuba, Ibaraki 305-0052, Japan

*Corresponding author. Tel.: +81 29 856 8622; Fax: +81 29 855 7240, Email address: yzaizen@mri-jma.go.jp (Y. Zaizen)

Asian dust samples were collected from the prefrontal and postfrontal air masses of an extratropical cyclone on 20 March 2010, and the size distributions and mixing properties of the mineral aerosols were examined by transmission electron microscopy and energy-dispersive X-ray analysis. Mineral aerosols were predominant in the large size ranges (Dp > 0.5 μm) in both samples. In the smaller size range (Dp < 0.5 μm), mineral particles dominated in the postfrontal samples, but particles with abundant sulfur were predominant in the prefrontal sample. Mixing properties of the mineral particles were examined by irradiation of individual particles by intense electron beams. In the postfrontal sample, most of the fine mineral particles were externally mixed, whereas most of those in the pre-frontal sample were internally mixed with volatile aerosols. The coating thickness depended on the core size. In particular, particles smaller than 0.3 μm were thickly coated. The mode diameters of mineral aerosols and of mineral cores were both in the fine size range of both dust samples. The aging properties of prefrontal dust and the strong influence of anthropogenic pollutants were due to the slow transport of the dust in the mixing layer over coastal China and the East China Sea. In contrast, the postfrontal dust was not particularly influenced by anthropogenic aerosols, because the front separated the air mass from the anthropogenic pollution south of the front.

Keywords: Aerosol particles; Asian dust; Single particle analysis; Electron microscope

1. Introduction

Asian dust particles affect human activities and health, plants, the environment, and climate. During dust events, fine particles are not important in terms of mass. However, observations at source regions suggest that the number concentrations of fine mineral particles are comparable to or higher than those of coarse mineral particles.

Aerosols in the fine size range are generally dominated by particles formed through gas-to-particle conversion, and they are thus composed of volatile materials, namely, sulfuric acid, sulfate, nitrate, ammonium, and organic matter. The number concentrations of these accumulation mode particles are generally several orders of magnitude higher than those of coarse particles. Therefore, number concentrations of fine mineral dust are expected to be lower than those of volatile particles even during Asian dust events over Japan.

During Asian dust events, mineral dust particles are typically transported in association with extratropical cyclones from the Asian continent to Japan. Dusty air is sometimes observed to be associated with northwesterly winds after the passage of a cold front, and increased particle concentrations are associated with southerly winds before the passage of a cold front [1, 2]. Increases in the number concentration of fine particles are particularly notable in prefrontal air masses, and they are attributable to anthropogenic pollution transported from China.

On 21 March 2010, Asian dust events were observed over Japan before and after the passage of a cold front. For the present study, we collected aerosol particles at Tsukuba during these events. We examined the mixing properties of the individual particles (examining approximately 10,000 particles) by observing morphological changes of the particles after their irradiation with strong electron beams during transmission electron microscopy (TEM).

2. Methods

Aerosol samples were collected with a two-stage jet impactor with nozzle diameters of 1 and 0.5 mm at flow rate of 2 L min^{-1} onto the surface of a carbon-coated nitrocellulose (collodion) film on a reference copper grid (Graticules, Ltd., Maxtaform H7). The 50% cutoff diameters of the

0.5-mm and 1-mm impactors were evaluated as 0.66 and 0.14 μm, respectively. The sampling sites were at the Meteorological Research Institute (MRI) in Tsukuba (36.08°N, 140.12°E) and at Mt. Haruna (36.48°N, 138.87°E; elevation, 1390 m).

The samples were analyzed by TEM (Hitachi, H-600 and H-6010), scanning TEM (STEM H-6010), and energy dispersive x-rays (EDX). Individual particles were irradiated by intense electron beams to remove volatile components such as sulfate, nitrate, and organic matter. Minerals and soot in the residues remaining after removal of the volatile materials were distinguished by their morphological appearance. The volatile aerosols were distinguished by the traces remaining after the irradiation. The size (volume equivalent diameter) of volatile aerosols was evaluated by assuming a spherical cap from the disk on the collection film.

3. Results and discussion

Figure 1 shows the number-size distributions of the different types of fine aerosol particles normalized to scanning mobility particle sizer/optical particle counter data (SMPS/OPC) for the prefrontal (left) and postfrontal (right) samples collected at Tsukuba. In the prefrontal event, externally mixed volatile aerosols predominated, and externally mixed refractory aerosols (minerals, soot, and fly ash) were present in very low concentrations. The refractory materials were mostly internally mixed with volatile aerosols. Number fractions of mineral particles were lower than 1%, even including the internally mixed particles.

Most soot particles were internally mixed. In the postfrontal event, the concentration of mineral aerosols was greater than the concentrations of soot and volatile particles in the 0.2–0.4 μm size range, and most mineral particles were externally mixed. It is notable that the maximum number concentration of total aerosols with a diameter of 0.4 μm was attributable to externally mixed mineral aerosols.

A model simulation showed that the source of the prefrontal and postfrontal dust was the Badain Jaran Desert (approximately 40°N, 100°E), a result that is consistent with back-trajectory analysis results. A dust storm was observed continuously at the meteorological observatories in that area from the beginning of March 2010. Therefore, we considered that the properties of the mineral particles in the prefrontal and postfrontal events were originally similar and that they became differentiated during transport. We interpreted the fine minerals in the prefrontal air to have been originally present as externally mixed particles, which became internally mixed under the influence of anthropogenic pollutants during transport.

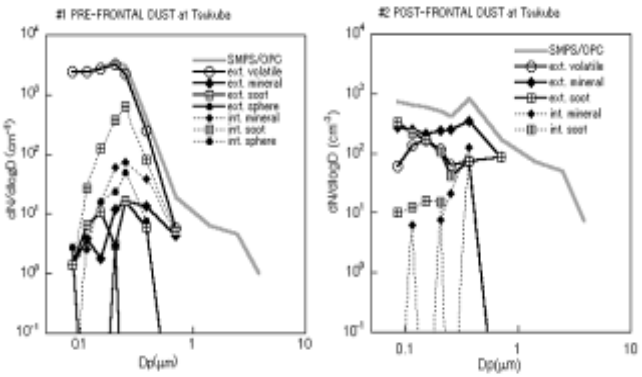

Figure 1 Size distributions of particles of different mixing types from the prefrontal (left) and postfrontal (right) events.

Bates et al. (2004: Ref. 1) observed aerosols from a research vessel in the Japan Sea near Sakhalin (approximately 50°N latitude) before and after the passage of a cold front accompanying an extratropical cyclone and reported that the prefrontal air was dominated by ammonium sulfate and organic carbon, with mineral dust particles as a minor component, whereas the postfrontal air was dominated by mineral dust particles. Zhang et al. (2005: Ref. 2) analyzed aerosol samples obtained at Qingdao, China, before and after the passage of a cold front passing over Mongolia (approximately 50°N latitude) and reported that the prefrontal dust had been highly influenced by anthropogenic pollution whereas the postfrontal dust was relatively unmodified. Moreover, some investigators have reported increased fine particle concentrations before the arrival of high concentrations of Asian dust in Japan. Taken together, these findings suggest that the effects of anthropogenic pollution on prefrontal air are generally stronger than their effects on postfrontal air.

1 Bates, T. S., P. K. Quinn, D. J. Coffman, D. S. Covert, T. Miller, J. E. Johnson, G. R. Carmichael, I. Uno, S. A. Guazzotti, D. A. Sodeman, K. A.Prather, M. Rivera, L. M. Russell and J. T. Merrill, 2004: Marine boundary layer dust and pollutant transport associated with the passage of a frontal system over eastern Asia. *Journal of Geophysical Research*, **109**, D19S19, doi: 10.1029/2003JD004094.

2 Zhang, D., Y. Iwasaka, G. Shi, J. Zang, M. Hu and C. Li, 2005: Separated status of the natural dust plume and polluted air masses in an Asian dust storm event at coastal areas of China. *Journal of Geophysical Research*. **110**, D06302, doi: 10.1029/2004JD005305.

Climatic effect of black carbon in the MRI global climate model

Taichu Y. Tanaka[1*] and MRI Earth System Modeling Group[*]

[1]Atmospheric Environment and Applied Meteorology Research Department, Meteorological Research Institute, 1-1 Nagamine, Tsukuba, Ibaraki 305-0052, Japan

Corresponding author. Tel.: +81 29 853 8621; Fax: +81 29 855 7240, Email address: yatanaka@mri-jma.go.jp (T. Y. Tanaka)

We used the global climate model MRI-CGCM3 to investigate the climatic effect of black carbon (BC) aerosols and to estimate the effectiveness of mitigation of global warming by the reduction of BC. As the first step, we conducted an idealized sensitivity study to investigate the climatic response of air temperature in the presence or absence of atmospheric BC aerosol, as well as the response with an atmospheric loading of BC 10 times that of the control experiment. We found that the atmospheric heating effect of BC was large in the tropical upper troposphere in mid-latitude regions of the Northern Hemisphere and in the Antarctic region. In addition, the surface air temperature in tropical regions, especially the Sahel, India, and Southeast Asia, was reduced by the presence of atmospheric BC. These results suggest that radiative heating of atmospheric BC modifies atmospheric stability conditions and hence the general circulation of the atmosphere and ocean.

Keywords: Black carbon; Climate change; Aerosol particles; Numerical climate model

1. Introduction

Black carbon (BC) in atmospheric aerosols is an efficient absorber of radiation, and it affects the Earth's climate by scattering and absorbing atmospheric radiation. BC is estimated to be the second-most important warming agent after carbon dioxide [1]. Moreover, when deposited on snow- or ice-covered ground, BC acts as a light-absorbing impurity and reduces the surface albedo (e.g. [2]). Because the lifetime of BC is shorter than that of other greenhouse gases (GHGs), reduction of atmospheric BC emissions may be an efficient way to mitigate global warming [1]. However, the climatic impact of BC is still uncertain because of the uncertainties in numerical climate models.

We used a global climate model developed in the Meteorological Research Institute (MRI) of the Japan Meteorological Agency to investigate the climatic effect of BC aerosols and to estimate the effectiveness of the mitigation of global warming by the reduction of BC. In section 2, we describe the MRI global climate model, and we present preliminary results of an experiment on the effect of BC aerosols in section 3.

2. Model description

2.1. MRI climate model

We used the global climate model MRI-CGCM3, which consists of an atmospheric general circulation model (MRI-AGCM3), an ocean general circulation model (MRI.COM), and a global aerosol model (MASINGAR mk-2; Model of Aerosol Species IN the Global Atmosphere) [3]. The horizontal resolution used was TL159 (approximately 1.1°) for the AGCM, 1° × 0.5° (tripolar) for the OGCM, and TL95 (approximately 1.8°) for the aerosol model. The vertical resolution of the AGCM and aerosol model was 48 vertical layers from the ground to 0.01 hPa with a terrain-following and pressure hybrid (η) coordinate system. The model components were interactively connected by a coupler library called Simple coupler (Scup, [4]). MRI-CGCM3 is a part of the MRI Earth System Model (MRI-ESM1) [5].

MASINGAR mk-2 considers five aerosol species, namely sulfate (and its precursors), BC, organic carbon (OC), sea salt, and mineral dust. The concentrations of the aerosols are passed to the AGCM and used for the calculation of atmospheric radiative transfer. Deposition fluxes of light-absorbing aerosols, namely BC and mineral dust, are also considered as snow impurities and used in the calculation of the albedo of snow and ice. Emission inventories of the Representative Concentration Pathways (RCP) emission scenario [6] are used for BC, OC, and SOx.

2.2. Experimental conditions

We performed a series of 25-year simulations for the period from 1 January 2005 to 31 December 2029, setting all GHG concentrations and BC, OC, and SOx emissions to those in 2005. The initial experimental conditions were adopted from a historical CMIP5 climate experiment

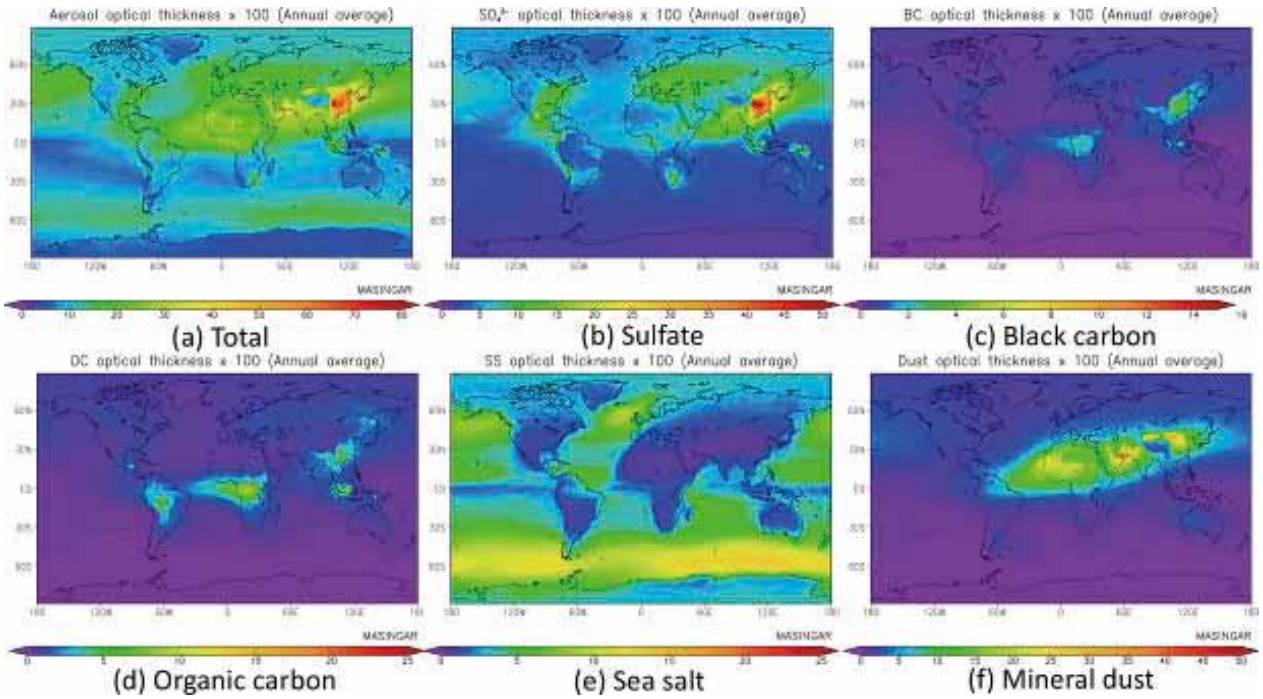

Figure 1 Annually averaged optical depth (at 550 nm) of the simulated aerosols: (a) total, (b) sulfate, (c) black carbon, (d) organic carbon, (e) sea salt, and (f) mineral dust.

conducted with MRI-CGCM3.

To elucidate the radiative effects of the BC aerosols, we conducted experiments under three sets of conditions. The default setup of the model simulation was used as the "Control" experiment. The second experiment (the "No-BC" experiment) excluded airborne BC from the radiative transfer calculation. The difference between the Control experiment and the No-BC experiment represented the effect of total elimination of BC emissions into the atmosphere. Because of uncertainties in the concentrations, mixing states, and optical properties in the BC simulation, as a sensitivity study we conducted a third experiment (the BC×10 experiment), in which the BC concentration was assumed to be 10 times the concentration in the atmosphere used for the Control radiative transfer calculation.

3. Results

3.1. Simulated optical depth of aerosols

The globally averaged annual mean optical depths of the aerosol species in the Control experiment (Figure 1) were 0.050 for sulfate, 0.003 for BC, 0.007 for OC, 0.042 for sea salt, and 0.029 for mineral dust. The horizontal distribution of the BC optical depth indicates that in the early 21st century BC loading will be highest over China, India, South-

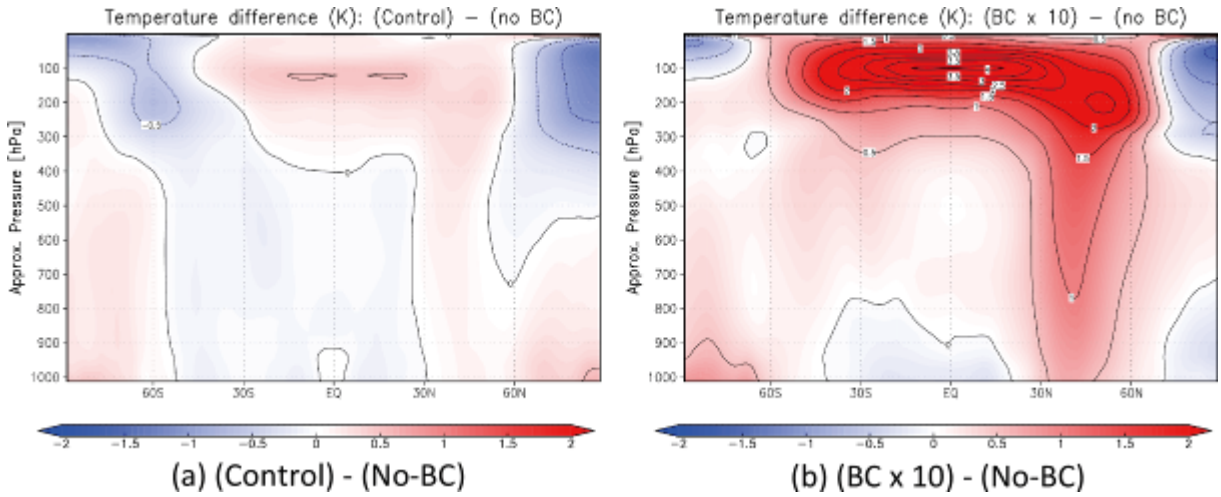

Figure 2 Annual mean zonally averaged temperature differences caused by the radiative effect of BC. Differences between the (a) Control and No-BC experiments and the (b) BCx10 and No-BC experiments.

east Asia, and the equatorial region in Africa. Most of the BC loading was in the Northern Hemisphere, and it was very low over the ocean in the Southern Hemisphere.

3.2. Zonal mean temperature differences

Zonal mean temperature differences between the Control and No-BC experiments (Figure 2a) show both positive and negative temperature anomalies, whereas those between the BC×10 and the Control experiments show positive temperature anomalies (Figure 2b) at most latitudes and altitudes.

In both experiments, a considerable positive temperature difference is present in the tropical upper troposphere, indicating BC heating there. In the middle and lower troposphere, negative temperature anomalies are seen from about 60°S to 30°N, suggesting that BC causes cooling of the lower troposphere at those latitudes.

Atmospheric heating in the presence of BC is also seen in mid-latitude regions of the Northern Hemisphere, where the BC loading is high, and positive temperature anomalies are found in the lower troposphere over the Arctic and Antarctic regions (Figure 2a), although in the upper troposphere and lower stratosphere, negative temperature anomalies are seen over the Arctic and Antarctic. However, the differences between the BC×10 and Control experiments indicate only a slight positive anomaly in the lower troposphere over the Antarctic and a slight negative anomaly over the Arctic (Figure 2b).

These results suggest that the presence of BC in the atmosphere affects large-scale atmospheric circulation. In the tropics, BC heats the upper troposphere and cools the lower troposphere, which should reinforce atmospheric stability and weaken convective transport.

3.3. Ground surface temperature differences

The annually averaged surface air temperature difference between the Control experiment and No-BC experiment (Figure 3a) suggests that with the current BC loading the surface air temperature will increase over northeastern China and Europe, where anthropogenic BC emissions are high. Also, surface air temperature in the presence of current BC loading is increased in Antarctic regions. In contrast, in low-latitude continental regions, especially the African Sahel, India, and Southeast Asia, surface air temperature differences show cooling with the current BC loading (Figure 3a). Moreover, more pronounced cooling tendencies are seen in these regions when the differences between the BC×10 and No-BC experiments are examined (Figure 3b).

In some regions, however, the current BC loading and the BC×10 loading show different tendencies when compared with the Control results. The considerable heating over the Arctic with the current BC loading (Figure 3a), compared with cooling over that region with BC×10 loading (Figure 3b), suggests that the effect of BC on surface temperatures in the Arctic region depends on the BC loading amount. In addition, the pattern of surface air temperature differences with respect to the No-BC experiment differs greatly over the ocean between the Control (Figure 3a) and BC×10 (Figure 3b) experiments. Large heating over the Antarctic in the latter experiment (Figure 3b) is attributable to a decrease in sea ice in that region. This result suggests that the surface air temperature change with the amount of BC loading is due to feedback from changes in the general circulation of the atmosphere and ocean induced by radiative heating due to the atmospheric BC loading.

3.4. Seasonal change in the global average surface temperature

The seasonal variation of the globally averaged ground surface temperature anomalies between the Control and No-BC experiments (Figure 4, blue line) suggests that globally averaged ground surface temperature from May to

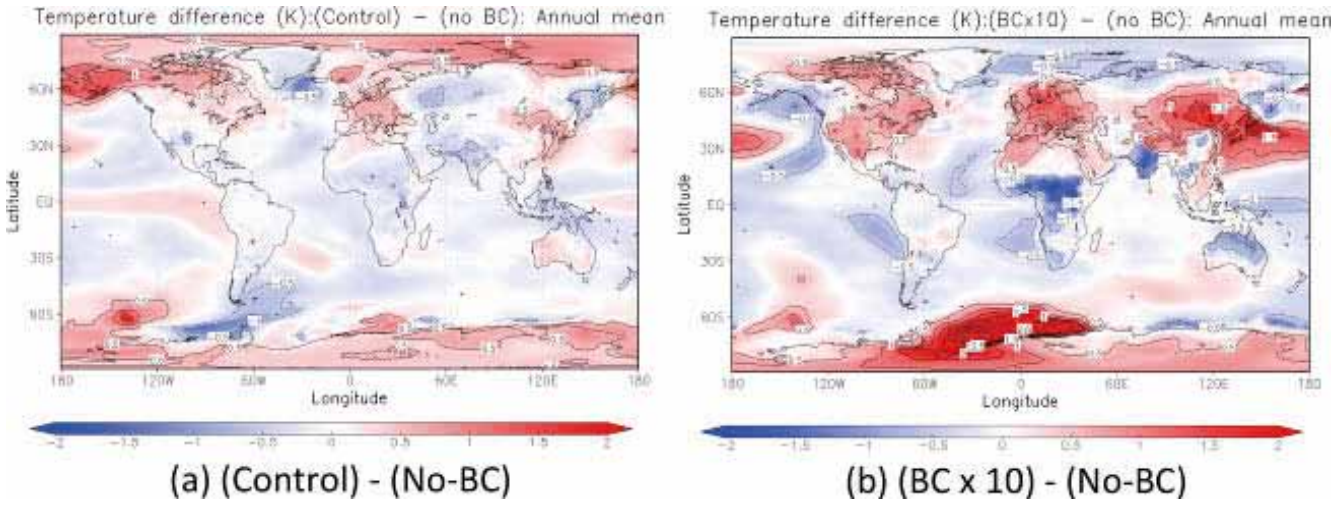

Figure 3 Annual mean surface air temperature differences due to the radiative effect of BC. Differences between the (a) Control and No-BC experiments, and the (b) BC×10 and No-BC experiments.

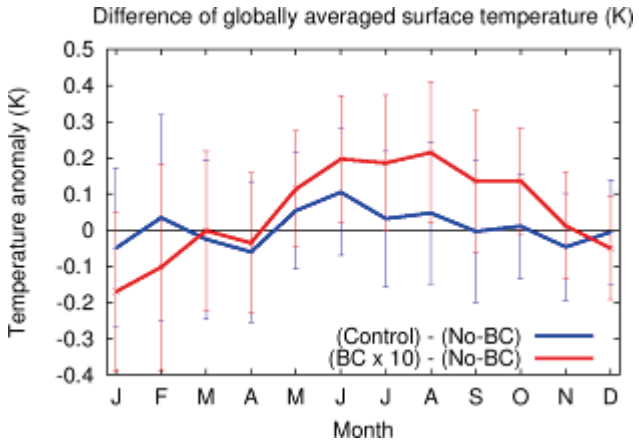

Figure 4 Seasonal variation of the globally averaged surface air temperature anomaly.

August will be slightly increased with the current atmospheric BC loading, whereas in autumn and winter, the globally averaged temperature anomalies are unremarkable. The heating due to BC in summer may reflect the large radiative heating due to BC in summer in the Northern Hemisphere, where there are large land masses and high anthropogenic BC emissions. The seasonal differences of the globally averaged surface air temperature anomalies between the BC×10 and No-BC experiments (Figure 4, red line) are greater than those between the Control and No-BC experiments; large positive anomalies (higher temperatures) are seen from May to October, and negative anomalies (lower temperatures) in January and December.

4. Summary

The global climate model MRI-CGCM3 was used to investigate the radiative effect of BC and to assess the validity of mitigating global warming by reducing atmospheric BC aerosol emission. As the first step of the assessment, we conducted an idealized sensitivity study to investigate the climatic response of air temperature in the presence or absence of atmospheric BC aerosols, and with an atmospheric BC loading 10 times higher than the current loading. The results predict a large atmospheric heating effect of BC in the tropical upper troposphere, mid-latitude regions of the Northern Hemisphere, and the Antarctic region in the early 21st century, and also suggest that surface air temperatures in tropical regions, especially the Sahel, India, and Southeast Asia, will be reduced by the presence of atmospheric BC. Therefore, radiative heating of atmospheric BC is predicted to change atmospheric stability conditions and hence the general circulation of the atmosphere and ocean. To assess regional temperature changes caused by BC reductions, more sensitivity experiments and investigations of feedback processes are needed.

This research was partly supported by the Environmental Research and Technology Development Fund (A-1101) of the Ministry of the Environment of Japan.

1 Jacobson, M.Z. 2002: Control of fossil-fuel particulate black carbon plus organic matter, possibly the most effective method of slowing global warming, *J. Geophys. Res.*, **107**, (D19), 4,410, doi: 10.1029/2001JD001376.

2 Aoki, T., K. Kuchiki, M. Niwano, Y. Kodama, M. Hosaka, and T. Tanaka, 2011: Physically based snow albedo model for calculating broadband albedos and the solar heating profile in snowpack for general circulation models, *J. Geophys. Res.*, **116**, D11114, doi: 10.1029/2010JD015507.

3 Yukimoto, S., Y. Adachi, M. Hosaka, T. Sakami, H. Yoshimura, M. Hirabara, T. Y. Tanaka, E. Shindo, H. Tsujino, M. Deushi, R. Mizuta, S. Yabu, A. Obata, H. Nakano, T. Koshiro, T. Ose, and A. Kitoh, 2012: A New Global Climate Model of the Meteorological Research Institute: MRI-CGCM3 —Model Description and Basic Performance —. *J. Meteorol. Soc. Japan*, **90A**.

4 Yoshimura, H. and S. Yukimoto, 2008: Development of a Simple Coupler (Scup) for Earth System Modeling. *Papers in Meteorology and Geophysics*, **59**, 19-29.

5 Yukimoto, S., H. Yoshimura, M. Hosaka, T. Sakami, H. Tsujino, M. Hirabara, T. Y. Tanaka, M. Deushi, A. Obata, H. Nakano, Y. Adachi, E. Shindo, S. Yabu, T. Ose and A. Kitoh, 2011: Meteorological Research Institute-Earth System Model Version 1 (MRI-ESM1) - Model Description - , *Technical Reports of the Meteorological Research Institute*, **No.64**, ISSN 0386-4049, Meteorological Research Institute, Japan.

6 Meinshausen, M., S. J. Smith, K.V. Calvin, J. S. Daniel, M. Kainuma, J.-F. Lamarque, K. Matsumoto, S.A. Montzka, S.C.B. Raper, K. Riahi, A.M. Thomson, G. J.M. Velders and D. van Vuuren, 2011: The RCP Greenhouse Gas Concentrations and their Extension from 1765 to 2300. *Climatic Change* **109**(1-2), 213-24

Model formulation and predictability of atmospheric aerosol properties and processes

Mizuo Kajino[1,*]

[1]Atmospheric Environment and Applied Meteorology Research Department, Meteorological Research Institute, 1-1 Nagamine, Tsukuba, Ibaraki 305-0052, Japan

Corresponding author. Tel.: +81 29 853 8623; Fax: +81 29 855 7240, Email address: kajino@mri-jma.go.jp (M. Kajino)

A new aerosol chemical transport model, the Regional Air Quality Model 2 (RAQM2), was developed to simulate Asian air quality. We implemented a simple version of a modal-moment aerosol dynamics model (MADMS) and achieved a completely dynamical (non-equilibrium) solution for gas-to-particle mass transfer over a wide range of aerosol diameters, from 1 nm to super μm. To consider a variety of atmospheric aerosol properties, a category approach was utilized: aerosols were distributed into four categories: Aitken mode (ATK), accumulation mode (ACM), soot aggregates (AGR), and coarse mode (COR). Condensation, evaporation, and Brownian coagulations for each category were solved dynamically. Modeled size distributions ($PM_{2.5}/PM_{10}$ and PM_1/bulk ratios) of total weight and chemical components were compared and found to be consistent with observations. At Hedo, proportions of non-sea-salt-SO_4^{2-} mixed with ATK + ACM were largest in summer, whereas H_2SO_4 gas was efficiently condensed onto AGR in cold seasons. Of the modeled NO_3^-, 98% was mixed with COR at Hedo, whereas 53.7% was mixed with sea salt at Gosan, which is upwind toward the Asian continent. This difference can be attributed to condensation of HNO_3 onto sea salt particles during transport over the ocean.

Keywords: Air quality modeling; Aerosol category approach; Non-equilibrium aerosol dynamics; Northeast Asia

1. Introduction

Atmospheric trace gases and aerosols have various detrimental effects on ecosystems and human health. Because their emission, secondary formation, transport, and deposition mechanisms are highly complex and still mainly unknown, many studies on the development and application of air quality modeling are ongoing. Recently, Jacobson and Ginnebaugh (2010: Ref. 1) developed a global-through-urban nested three-dimensional air pollution model that implements a large explicit photochemical mechanism with 4675 gases and 13,626 tropospheric and stratospheric chemical reactions. The mechanism also includes one internally mixed aerosol and three hydrometeor categories that are size and chemistry resolved (17 components and 14 size bins for aerosols; 18 components and 30 size bins for cloud/precipitation liquid, cloud/precipitation ice, cloud/precipitation graupel). On the other hand, there is still a strong demand for computationally efficient models for the purpose of long-term integration with higher grid resolutions. For example, the Community Multiscale Air Quality (CMAQ) model [2] has been extensively used, and continually updated, worldwide for more than 10 years; the current version is 4.7 [3].

Asian air quality is highly complex because Asia covers regions from the tropics to the polar zones with huge amounts of anthropogenic air pollutants and natural dust particles together with other natural species. The Regional Air Quality Model (RAQM) was developed at the Acid Deposition and Oxidant Research Center (now called the Asia Center for Air Pollution Research), which focuses on such Asian air quality problems [4, 5]. RAQM has been used for various air pollution studies in Asia, such as studies on high-oxidant, massive dust transport, and volcanic sulfur events, and it has been substantially modified by means of comparisons and evaluation with extensive and long-term monitoring data [4, 5] and with other models ([6] and references therein). However, an aerosol dynamics module was not implemented in RAQM, and thermodynamic equilibrium was assumed for gas–aerosol partitioning of semi-volatile inorganic components such as sulfate, nitrate, and ammonium.

To simulate the evolutionary processes of aerosol microscale properties such as chemical composition, size distribution, and mixing state, we implemented a simple ver-

sion of a new modal-moment aerosol dynamics model [7-9] that enables the non-equilibrium calculation of gas-to-particle mass transfer for a wide range of aerosol diameters from 1 nm to super μm. We also implemented six important parameterizations relating to aerosol dynamics: (1) new particle formation, (2) cloud condensation nuclei activation, (3) ice nuclei activation, (4) an explicit grid-scale cloud microphysical module, (5) dry deposition, and (6) sub-grid-scale convection and scavenging. This new model is called RAQM2. In this report, only the general findings of the study are summarized. A detailed description of the model and further details of our findings are presented by Kajino et al. (2012a: Ref. 10, 2012b: Ref. 11).

2. Methods

The model framework is illustrated in Figure 1. The U.S. National Center for Environmental Prediction (NCEP) 6 h, 1° final operational global analysis data set ds083.2 (http://rda.ucar.edu/datasets/ds083.2/), the Japan Meteorological Agency (JMA) Climate Data Assimilation System data set (JCDAS, 6 h, 1.25°, http://jra.kishou.go.jp/JRA-25/AboutJCDAS_en.html), or the JMA Meso Regional Objective Analysis (MANAL) data set (3 h, 5 km) are used for the initial and boundary conditions of the global and regional meteorological model simulations and also for the analysis nudging method. The Advanced Research Weather Research and Forecasting (WRF) model or the JMA nonhydrostatic model (NHM) are used to simulate the regional-scale meteorological field. In this study, WRF was selected as the regional model and it was driven by NCEP ds083.2.

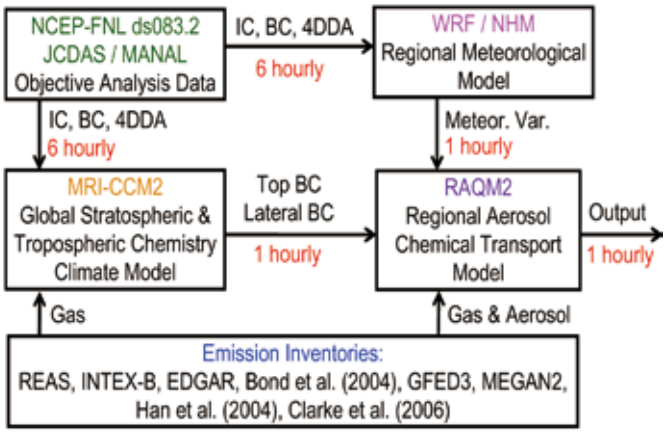

Figure 1 Framework of the RAQM2 system

The model domain, common to both WRF and RAQM2, is illustrated in Figure 2, which also shows locations of observation sites of the Acid Deposition Monitoring Network in East Asia (EANET). The horizontal grid resolution is 60 km with a Lambert conformal map projection; vertically there are 28 layers from the ground to 100 hPa for WRF, and 13 layers from the ground to 10 km for RAQM2, with terrain-following coordinates. The output time interval of the WRF was set to 1 h, and thus the input/output time interval for RAQM2 was also 1 h.

We used EANET monitoring data (Guidelines for acid deposition monitoring in East Asia, available at http://www.eanet.cc/product.html) for model evaluation. The EANET stations monitor 1- or 2-week accumulated concentrations of gaseous species and aerosol components using the filter pack (FP) method (Technical documents for the filter pack method in East Asia; http://www.eanet.cc/product.html). These stations monitor hourly concentrations of air pollutants and meteorological data such as wind speed, wind direction, temperature, relative humidity, and solar radiation.

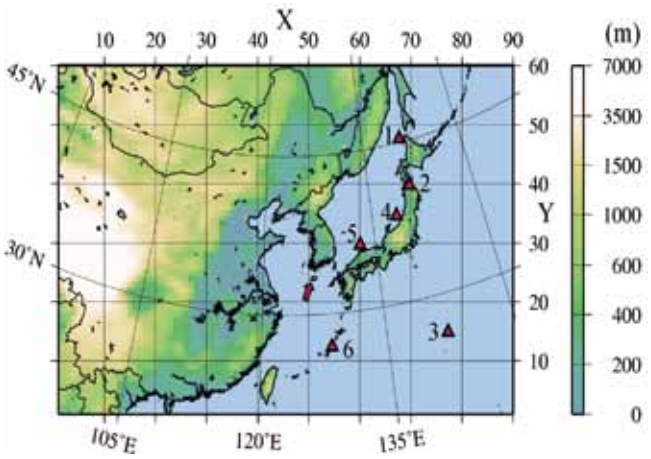

Figure 2 Model domain showing terrestrial elevation (m) and six Japanese EANET sites (1, Rishiri; 2, Tappi; 3, Ogasawara; 4, Sado; 5, Oki; 6, Hedo). The arrow indicates the Gosan site on Jeju Island, Korea.

Six EANET stations located on small islands or on isolated capes in the downwind region in Japan were selected for the model evaluation (Figure 2, red triangles). These stations have no nearby large anthropogenic emission sources and lack the complexity of local orographically induced winds. Therefore, air pollutant transport events mostly coincided with synoptic-scale disturbances at these stations and are generally well reproduced by regional-scale models. On the other hand, because the stations are very close to ocean surfaces, regional-scale simulations of ocean-originated species such as sea salt often do not agree well with the observations. Thus, we often obtain a better agreement for sea salt-originated components at inland or mountainous stations.

3. Results and discussion

Statistical analyses by Kajino et al. (2012a: Ref. 10). showed that the model reproduced the regional-scale transport and transformation of the major inorganic anthro-

pogenic and natural air constituents within factors of 2 to 5.

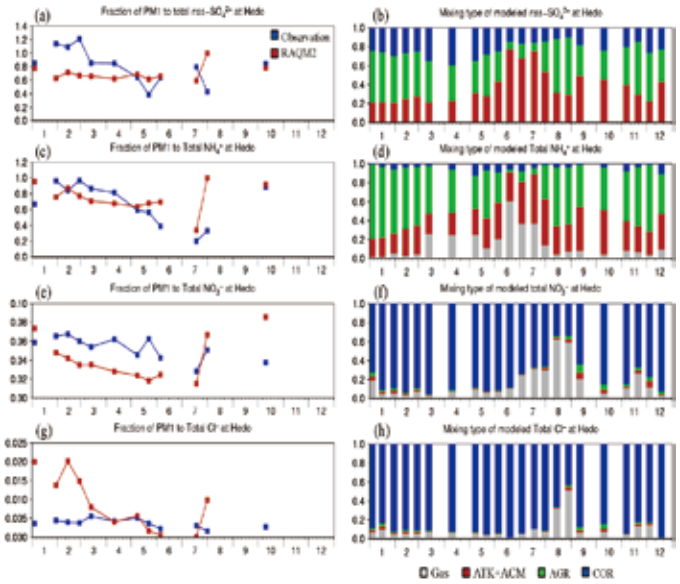

Figure 3 Biweekly mean PM_1 to total (gas plus aerosol) concentration ratios (left) and modeled fractions of the gas phase (gray) and aerosol categories ATK+ACM (red), AGR (green), and COR (blue) (right) at Hedo: (a), (b) nss-SO_4^{2-}; (c), (d) T-NH_4^+; (e), (f) T-NO_3^-; and (g), (h) T-Cl^-.

Figure 3 summarizes the major findings of the study at Hedo. The observed values are depicted only when the available hourly aerosol mass spectrometer data exceeded 50% during each biweekly FP sampling period (more than 140 hourly data during two weeks). The observed median PM_1 to bulk non-sea-salt (nss)-SO_4^{2-} ratio was 0.85. The ratio exceeded 1.0 in some cases, so it may be within the uncertainties of the analysis (Figure 3a). The modeled ratio was also large because approximately 80% of the nss-SO_4^{2-} was mixed with submicron particles, such as ATK, ACM, and AGR (Figure 3b). The modeled median ratio was 0.66, smaller than the observed ratio, indicating that the modeled size distribution of nss-SO_4^{2-} may have been larger than the observed distribution, or the proportions mixed with larger COR particles might have been overestimated. The features of the NH_4^+ ratio were similar to those of the nss-SO_4^{2-} ratio because nss-SO_4^{2-} is a major counterpart of NH_4^+. The proportion of total NH_4^+ (T-NH_4^+) in the gas phase, as NH_3, ranged from 20% to 60% in summer, because the temperature was high enough for NH_4NO_3 to evaporate and/or because the amount of nss-SO_4^{2-} was not enough to take up NH_3 gas and fix it to the aerosol phase as ammonium sulfate. Because the modeled nss-SO_4^{2-} and NH_4^+ were both underestimated, improvement of nss-SO_4^{2-} could also result in improvement of NH_4^+.

The mixing type of NO_3^- at Hedo was interesting in comparison with that at Gosan, Jeju Island, Korea. The observed and modeled median PM_1 to total NO_3^- (T-NO_3^-) ratios were 0.054 and 0.035, respectively, more than one order of magnitude smaller than those of nss-SO_4^{2-} and NH_4^+. This result means that the observed and modeled T-NO_3^- partitioned into the gas phase or internally mixed with aerosols larger than PM_1 were close to each other, at 94.6% and 96.5%, respectively. Kajino and Kondo [9] conducted a similar analysis of the $PM_{2.5}/PM_{10}$ ratios of chemical components at Gosan and calculated that on average 53.7% of the modeled NO_3^- was internally mixed with sea-salt particles in March 2005. This value was consistent with observations; the mean modeled and observed $PM_{2.5}/PM_{10}$ ratios of NO_3^- were both 0.66. In the current simulation, 98% of the NO_3^- was internally mixed with COR, based on the annual average at Hedo (Figure 3f).

During long-range transport, HNO_3 gas is produced via photochemical oxidation of NO_x. The mass transfer coefficients for each aerosol category are nearly proportional to their total surface area for atmospheric aerosol size ranges (free-molecular regime). Over the continent, more than 90% of the NO_3^- was mixed with submicron particles as NH_4NO_3. In contrast, over the ocean, toward downwind regions of the continent, HNO_3 gas produced during transport is more efficiently condensed onto sea-salt particles, because the proportions of sea-salt surface area become large.

Gosan is located approximately 700 km upwind of Hedo, in the direction of the Asian continent. The spatial distributions of the mixing types of NO_3^- showed that more than 90% of the NO_3^- could be internally mixed with sea salt over regions further downwind such as Hedo, whereas approximately 50% was mixed with sea salt over the Yellow Sea, where Gosan is located (Figure 6l of [9]).

Kajino et al. (2012b: Ref. 11) also evaluated model system performance regarding the major inorganic components of rain and snow precipitation measured at EANET stations. Statistical analysis showed that the model system successfully reproduced the regional-scale emission, transport, transformation, and wet deposition processes of major inorganic components of both anthropogenic and natural species, such as nss-SO_4^{2-}, NH_4^+, NO_3^-, Na^+ and nss-Ca^{2+}. Interestingly, however, we found that only modeled Na^+ in precipitation at near-coast stations was significantly underestimated (by a factor of up to 30), which suggests that the contribution of short-lived, super-large sea-salt droplets (SLSD; D = ~10–100 μm) was substantial in precipitation samples at near-coast stations in Japan (150–700 m from the coast). SLSD can be transported horizontally from the coast about 1–10 km, which means that the horizontal representativeness of the wet deposition of sea-salt-originated components such as Na^+ and Cl^- is limited to that transport distance. However, SLSD are not collected when aerosols are sampled by the FP method, because SLSD settle rapidly and they do not enter the air intake with the low pumping flow rate of 1 L min^{-1}. Therefore, the horizontal representativeness of Na^+ and Cl^- concentrations in air concentrations can be adequately large as the traveling distance of the coarse

mode particles (>100 km).

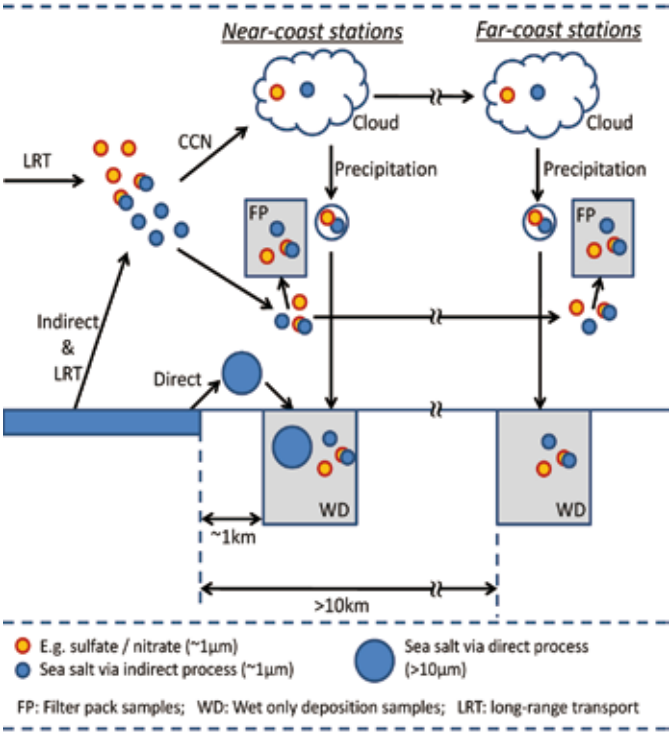

Figure 4 Schematic illustration showing the possible effects of super-large sea-salt droplets (SLSD) on wet deposition samples at near-coast stations.

These processes are summarized in Figure 4. The outcome of our study gives an important perspective on pH values of precipitation at Japanese EANET stations. Seawater pH is about 8, much higher than the pH of precipitation (~5). Thus, the pH of precipitation at near-coast stations might be increased by contamination with SLSD. However, a simple calculation suggests that the effect of SLSD on precipitation pH is very low, about 0.014 pH units on average if the SLSD fraction of sea salt in precipitation is assumed to be 90%.

4. Conclusion

A new aerosol chemical transport model, the Regional Air Quality Model 2 (RAQM2), was developed to simulate Asian air quality. A regional-scale simulation (Δx = 60 km) was performed for the entire year of 2006 covering the northeast Asian region. Statistical analyses showed that the model successfully reproduced the regional-scale transport, transformation, and wet deposition of the major inorganic anthropogenic and natural air constituents.

The modeled mixing types of the chemical components were found to be interesting, but the results were not compared with direct measurements of the mixing state. These results should be evaluated in the future by comparing them with measurements of soot mixing states made by volatility tandem differential mobility analyzer, single particle soot photometer, or transmission electron microscopy analyses. The aerosol mixing type is a key parameter influencing the light-scattering and absorbing properties of the aerosol. Further investigations are needed that compare our results with aerosol optical thickness or single scattering albedo observations for accurate assessment of aerosol–radiation interaction processes.

This research was supported by the Fundamental Research Budget of the Meteorological Research Institute of Japan, "Studies on Atmospheric Aerosol Properties and Processes". The study was partly supported by the Environmental Research and Technology Development Fund (Project No.B-0905 and A-1101) of the Ministry of the Environment of Japan. Aerosol mass spectrometer data for Hedo were provided by Dr. A. Takami at the National Institute for Environmental Studies and Prof. S. Hatakeyama at the Tokyo University of Agriculture and Technology.

1 Jacobson, M. Z. and D. L. Ginnebaugh, 2010: Global-through-urban nested three-dimensional simulation of air pollution with a 13,600-reaction photochemical mechanism. *J. Geophys. Res.*, **115**, D14304.

2 Byun, D. and K. L. Schere, 2006: Review of the governing equations, computational algorithms, and other components of the Models-3 Community Multiscale Air Quality (CMAQ) Modeling System, *Applied Mechanics Reviews*. **59**, 51-77.

3 Foley, K. M., S. J. Roselle, et al. 2010: Incremental testing of the Community Multiscale Air Quality (CMAQ) modeling system version 4.7, *Geosci. Model Dev.*, **3**, 205-226.

4 An, J., H. Ueda, et al. 2002: Simulations of monthly mean nitrate concentrations in precipitation. *Atmos. Environ.*, **36**, 4,159-4,171.

5 Han, Z., 2007: A regional air quality model: evaluation and simulation of O_3 and relevant gaseous species in East Asia during spring 2001, *Environ. Modell. Softw*. **22**, 1,328-1,336.

6 Carmichael, G. R., T. Sakurai, et al. 2008: MICS-Asia II: the model intercomparison study for Asia phase II methodology and overview of findings, *Atmos. Environ.*, **42**, 3,468-3,490.

7 Kajino, M., 2011: MADMS: Modal Aerosol Dynamics model for multiple modes and fractal shapes in free-molecular and near-continuum regimes. *J. Aerosol Sci.*, **42**, 224-248.

8 Kajino, M. 2011: Development of an efficient but accurate new dynamics model to predict a variety of atmospheric aerosol properties and their elemental processes, *Earozoru Kenkyu*. **26** (4) 296-306 (in Japanese).

9 Kajino, M., Y. Kondo, 2011: EMTACS: Development and regional-scale simulation of a size, chemical, mixing type, and soot shape resolved atmospheric particle model. *J. Geophys. Res.*, **116**, D02303, doi: 10.1029/2010JD015030.

10 Kajino, M., Y. Inomata, et al. 2012a: Development of an aerosol chemical transport model RAQM2 and predictions of Northeast Asian aerosol mass, size, chemistry, and mixing type. *Atmos. Chem. Phys. Discuss.*, **12**, 13,405-13,456, doi: 10.5194/acpd-12-13405-2012.

11 Kajino, M., M. Deushi, et al. 2012b: Modeling rain and snow precipitation quality over Northeast Asia using MRI-PM/c and implications of super large sea salt droplets effects at near-coast stations. Geosci. *Model Dev. Discuss*. **5**, 1,341-1,379, doi: 10.5194/gmdd-5-1,341-2,012.

Aerosol-related services of the Japan Meteorological Agency

Hiroki Shiozuru[1*], Nozumu Ohkawara[1], Kensuke Ishii[1] and Akinori Ogi[1]

[1]Aerosol Observation Section, Atmospheric Environment Division, Global Environment and Marine Department, Japan Meteorological Agency, 1-3-4 Otemachi, Chiyoda, Tokyo 100-8122, Japan

**Corresponding author. Tel.: & Fax: +81 3 3212 8341 (ext.4762); Email address: shiozuru@met.kisho.go.jp (H. Shiozuru)*

The Atmospheric Environment Division, Japan Meteorological Agency (JMA), is in charge of monitoring global/regional aerosols and issuing information about them. Our main products are as follows:

1) Measurement data of aerosol optical depth (AOD) by sun photometer

We operate three observational sites to measure AOD: Ryori in northern Japan since 1988; Minamitorishima in the northwestern Pacific since 1995; and Yonagunijima in the southwestern islands since 1998. In 2002, the measurement instrument at Ryori was upgraded to a precision filter radiometer and in 2007 the instruments at Minamitorishima and Yonagunijima were upgraded. Monthly mean AOD at those stations are published in the "Annual Report on Atmospheric and Marine Environment Monitoring."

2) *Kosa* (aeolian dust) information

In spring, Japan is frequently affected by *Kosa* from the Eurasian continent. We present the current and expected risk of K*osa* to the public by providing information about visibility at meteorological observation stations and forecasts of dust concentrations through the JMA website. The dust forecasts are derived by using the MASINGAR numerical dust forecast model, which was developed at the Meteorological Research Institute/JMA to study global atmospheric aerosols and related trace species.

3) Satellite aerosol monitoring products

The Meteorological Satellite Center of JMA retrieves aerosol products from the visible and infrared channels of the Geostationary Meteorological Satellite (MTSAT). The aerosol optical thickness is determined for the area from 52°N to 17°N and 114°E to 150°E. We also monitor aerosols using products derived from Earth Observation Satellites such as Aqua and CALIPSO.

4) Global Aerosol Optical Depth climatology for the numerical weather prediction (NWP) model

We processed AOD data derived from MODIS on Terra (2000–2005) and AOD data from MODIS on Terra and Aqua (2000–2008) to create a global monthly AOD climatology. This product is used in the JMA's operational global NWP model to improve the radiation-aerosol interaction.

Keywords: Aerosol optical depth; *Kosa* (Asian dust) forecasts; Retrieved satellite products; Japan Meteorological Agency